Technical

Report

Interim Report
I-C2028-1

THE APPLICATION OF HYDRODYNAMIC GREASE LUBRICATED SELF-SEALING BEARINGS TO A GYRO SPIN AXIS: A FEASIBILITY STUDY

By

J. T. McCabe
F. Kramberger

January 1968

Prepared for

NATIONAL AERONAUTICS AND SPACE ADMINISTRATION
George C. Marshall Space Flight Center
Huntsville, Alabama

THE FRANKLIN INSTITUTE RESEARCH LABORATORIES
BENJAMIN FRANKLIN PARKWAY • PHILADELPHIA, PENNA. 19103

Technical

Report

Interim Report
I-C2028-1

THE APPLICATION OF HYDRODYNAMIC GREASE LUBRICATED SELF-SEALING BEARINGS TO A GYRO SPIN AXIS: A FEASIBILITY STUDY

By

J. T. McCabe
F. Kramberger

January 1968

Prepared for

NATIONAL AERONAUTICS AND SPACE ADMINISTRATION
George C. Marshall Space Flight Center
Huntsville, Alabama

THE FRANKLIN INSTITUTE RESEARCH LABORATORIES
BENJAMIN FRANKLIN PARKWAY • PHILADELPHIA, PENNA. 19103

FOREWORD

This report was prepared in accordance with National Aeronautics and Space Administration Contract NAS8-20741 with William J. McKinney acting as Contracting Officer, Carl H. Mandel, Principal, John L. Burch as Alternate. Monthly progress reports were transmitted to Daniel V. Finnegan, RR-RC and technical liaison was conducted through John L. Burch.

J. T. McCabe acted as Project Engineer for FIRL. Frank Kramberger supervised the experimental phase of the program. Additional engineering assistance was provided by Jim Dunfee, design; Dr. T. Y. Chu, analysis; Frank Rush and Charles Stevenson, computation. Test rig machine work was performed by John Stuprick with guidance from Ed Jones and Frank Kramberger.

John T. McCabe
Project Engineer

Frank Kramberger
Technical Associate

Approved by:

O. Decker, Manager
Friction and Lubrication

Z. Zudans
Technical Director

Interim Report I-C2028-1
The Application of Hydrodynamic
Grease Lubricated Self-Sealing
Bearings to a Gyro Spin Axis:
A Feasibility Study

By

J. T. McCabe and Frank Kramberger
Franklin Institute Research Laboratories
January 1968

For

National Aeronautics and Space Administration,
George C. Marshall Space Flight Center
Contract NAS8-20741

ABSTRACT

This report is concerned with the application of grease lubricated spiral groove bearings to a gyro spin axis. It contains performance characteristics for the spherical and conical configurations, the analysis used in obtaining these characteristics, an experimental check on the analysis and details on the experimental test facilities that were constructed for feasibility confirmation.

Information is also presented on the properties of a lubricant selected from an experimental screening study.

Results of the program indicate that a grease lubricated conical bearing with spiral grooves is feasible for certain gyro spin axis applications.

TABLE OF CONTENTS

TABLE OF CONTENTS (CONT.)

LIST OF FIGURES

LIST OF FIGURES (CONT.)

LIST OF FIGURES (CONT.)

LIST OF TABLES

1. INTRODUCTION

The main purpose of this study is to determine the practicality of building a sophisticated prototype gyro assembly with a 24,000 RPM spin rotor supported by *hydrodynamic fluid film self-sealing bearings*. The total power available is 8 watts; the rotor and bearing available space, a volume approximated by a 2 inch diameter sphere.

For the most part, present day gyro spin axes are supported by ball bearings. High load capacity, ruggedness and ready availability through several sources are inherent advantages of ball bearings. Moreover, they can be made nearly isoelastic and relatively cheap. They also provide good rotor stability, even while operating in a vibrating environment. On the other hand, the balls themselves introduce vibrations and a "good" set of gyro bearings cannot be preselected from a batch of bearings even though a high standard of quality control is maintained. The failure mode for these ball bearings is judged on the basis of operating torque. Thus, the gyro must be at least partially assembled before a final evaluation can be made.

To reduce operating torque, vibration and increase long term reliability, part of the recent gyro development effort has shifted to the study and testing of hydrodynamic full fluid film spin axis bearings using the gas in the wheel cavity as the lubricant. Gas bearing eliminate the lubricant supply and migration problems while still providing full separation of the bearing surfaces. Potentially, the result is a long running life and the elimination of rolling element vibration. Among their disadvantages may be numbered poor boundary lubrication, potential whirl instability, low load capacity, high manufacturing cost and questional performance characteristics in a vibrating environment.

In the present study, grease is substituted for the gas. In all cases studied, the grease is hydrodynamically pressurized by rotating spiral grooves. Most of the advantages of the gas lubricant are retained with the exception of those associated with maintaining the physical and

chemical properties of the lubricant. These problems will require further development but they are not considered insurmountable.

In comparison with a gas, a grease lubricant has the added advantage of high film damping, high load capacity, and excellent boundary lubrication. Also, low bearing friction loss can be achieved because load dictated bearing dimensions are small. Thus surface speed is low. In addition, reducing the wheel cavity pressure will lower windage losses.

Ample reasons for exploiting the advantages offered by grease lubricated spiral groove bearings appear to be readily apparent. In a gyro application requiring stop-start reliability over a long period of time and a relatively short duty cycle, this is especially true.

2. SUMMARY

The following items have been completed under the present contract:

2.1 Justification for the selection of either spherical or conical "dead ended" grease or oil lubricated spiral groove bearings for a gyro spin axis.

2.2 Development of theoretical analyses for determination of the performance characteristics of spherical and conical bearings.

2.3 Development of digital computer programs to impliment the above analyses.

2.4 A non-dimensional parametric study of the spherical and conical bearing configurations for partial optimization and mutual comparison.

2.5 The selection of the conical configuration as the most promising candidate for the gyro spin axis.

2.6 A determination of the theoretical specicifications and performance characteristics of a grooved conical bearing for isoelastic response and maximum load capacity.

*2.7 Fabrication of a Single Bearing Test Rig for partial confirmation of the theoretical analysis and for screening potential lubricants.

2.8 Selection of the properties of a suitable grease lubricant by torque and film temperature vs. load tests on the Single Bearing Test Rig.

---

* This rig was constructed in parallel with the execution of the NASA program as an FIRL in-house sponsored project.

2.9 Fabrication of the grooved shaft and mating conical bearing as specified by the analysis.

2.10 The design and fabrication of a precise test rig simulating the gyro rotor and spin axis bearings. This rig measures rotor speed torque, displacement and dynamic responce.

2.11 Development of a rig and technique for balancing the gyro rotor.

2.12 Experimental measurements of load vs. bearing power consumption and load vs. rotor displacement for the grease lubricated spiral groove spin axis bearing.

3. CONCLUSIONS AND RECOMMENDATIONS

The following conclusions can be made as a result of this program:

3.1 The analysis and experimental testing done to date indicate that a grease lubricated spiral groove bearing of the dead-ended conical configuration (truncated cone) is feasible for use as a spin axis bearing.

3.2 High load capacity, low compliance, good start-stop characteristics and low bearing power consumption are possible.

3.3 Although it appears possible to satisfy the operating specifications equally as well with the spherical configuration, the conical configuration provides more design latitude and is easier to fabricate. The conical configuration is recommended for further study.

3.4 Since only short term tests were performed, the feasibility of using grease lubricated spiral groove bearings for applications requiring negligible lubricant migration and negligible loss of physical and chemical lubricant properties over a long period has not yet been proven.

3.5 Consideration must be given to the machinery used to fabricate the bearing components because of small bearing dimensions. Specialized machinery with highly accurate spindles and support bearing may have to be constructed.

3.6 Materials must be selected that are capable of taking a fine finish and maintaining dimensional stability if very low compliance is to be achieved.

The following recommendations are made as a result of this program:

3.7 A two phase program should be undertaken to develop a suitable lubricant. One phase should be directed towards determining the gross properties of a "good" lubricant for *immediate* use. This work should be accomplished in a relatively short time using commercially *available* stock and should produce a lubricant that is at least acceptable for short term testing. The other phase should be directed at the *development* of a lubricant that is capable of maintaining its physical and chemical properties over a period of at least two years.

3.8 Experimental optimization studies should be undertaken for the conical bearing. This would provide confirmation for the analysis and aid in judging the trade-off between the analytical indicated optimum design and fabrication difficulties. The specification of machine tool requirements for conical bearing fabrication should also be made a part of this study.

3.9 The analysis that was used in the feasibility should be improved. This analysis was based on Reference 1 and contains certain assumptions that were considered acceptable for a feasibility study but can be eliminated by a more comprehensive treatment.

3.10 The basic cone design should be modified to minimize lubricant migration and to promote the maintainance of its physical and chemical properties. One possibility is to continuously circulate the lubricant in the bearing.

3.12 A prototype gyro assembly should be built with the spin rotor supported by the grease lubricated bearing given in the Design Summary section of this report. This undertaking would complement the program outlined above by critically evaluating the design data as it is made available.

4. DESIGN SUMMARY AND PERFORMANCE DATA

4.1 Performance Specifications

The performance specifications representing the ultimate goal for the grease lubricant gyro prototype are:

- Rotor weight - 2.81 Newtons
- Rotor speed in helium atmosphere - 24,000 rpm
- Rotor power - 8 watts
- Rotor angular momentum 2.6×10^{-6} g cm^2/sec
- Maximum design load - 6 g
- Slew rate - 1 radian per second
- Maximum mass shift - 1/2 dyne cm
- Working life - 2 years with 1000 stops and starts

4.2 Design Specifications

Under the present contract, no attempt was made to run the rotor in helium, to slew the rotor, to measure mass shift or to perform 1000 stop-start tests. Emphasis was placed on determining the bearing load-deflection-torque characteristics.

Based on the analysis, the design specifications of a cone bearing that will meet the load-power requirements are as follows (see Fig. 4.1):

- Base diameter of Cone, 2R = 3/16 in.
- Number of leads, N = 6
- Half cone angle, $T_A = 30° \pm 1°$
- Length to radius ratio, $L/R = 1 \pm 0.1$
- Land to groove width ratio, $\gamma = 0.9 \pm 0.1$
- Groove angle, $\alpha = 12° \begin{smallmatrix} + 3° \\ - 2° \end{smallmatrix}$

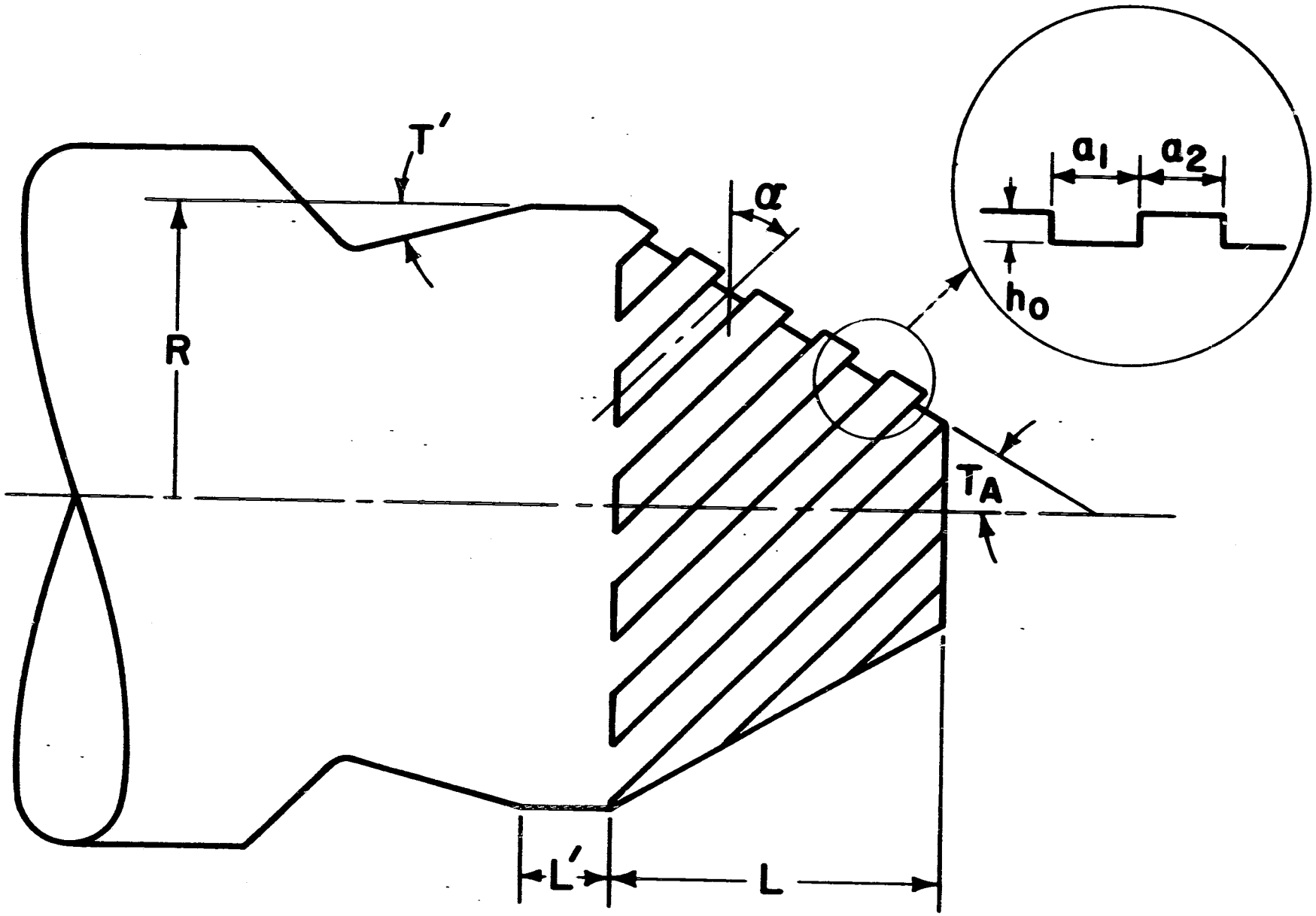

FIG. 4-1 GEOMETRY OF SPIRAL GROOVE CONICAL JOURNAL

- Lubricant viscosity, $\eta = 5 \times 10^{-6} \pm 2 \times 10^{-6}$ lb sec/in.^{2} at 1 g operating temperature
- Maximum deviation between cone land surface and socket surface = 20 microinches
- Flat length L' = 0.025 in.
- Slinger angle T' = 15°

Figure 4.2 shows the grooved journal that was fabricated at FIRL to meet the above specifications. The rotor consists of three components; two shaft segments, each similar to Figure 4.2, and a disc with machined in buckets. The mating bearing surface consistes of a simple dead-ended cone machined by a shaped tool to the same angle as the journal cone.

4.3 Theoretical Performance Data

Figures 4.3 through 4.7 give the theoretical performance data for the cone bearing. These data were obtained using the analysis outlined in Section 5. All curves are based on the use of a lubricant with an "apparent" viscosity of 5×10^{-6} lb sec/in.^{2}; the abscissa is "y", the axial separation of the male and female cones. When y = o, and the cones are concentric, the bearing clearance is zero. Since the "included" cone angle for these plots of 60°, the *concentric clearance* measured perpendicular to the bearing surfaces is y/2. The coordinate "x" measures radial displacement from the center line of the stationary bearing.

Table 4.1 shows a schedule of potential operating conditions intended for checking the present theory with experimental measurements. In all cases, a relatively large minimum clearance is used to minimize the influence of measurement errors. With precision machining and assembly, an operating clearance of 0.0001 is possible. At this clearance, the axial compliance would be about 6 micro inches/lb for the design described above.

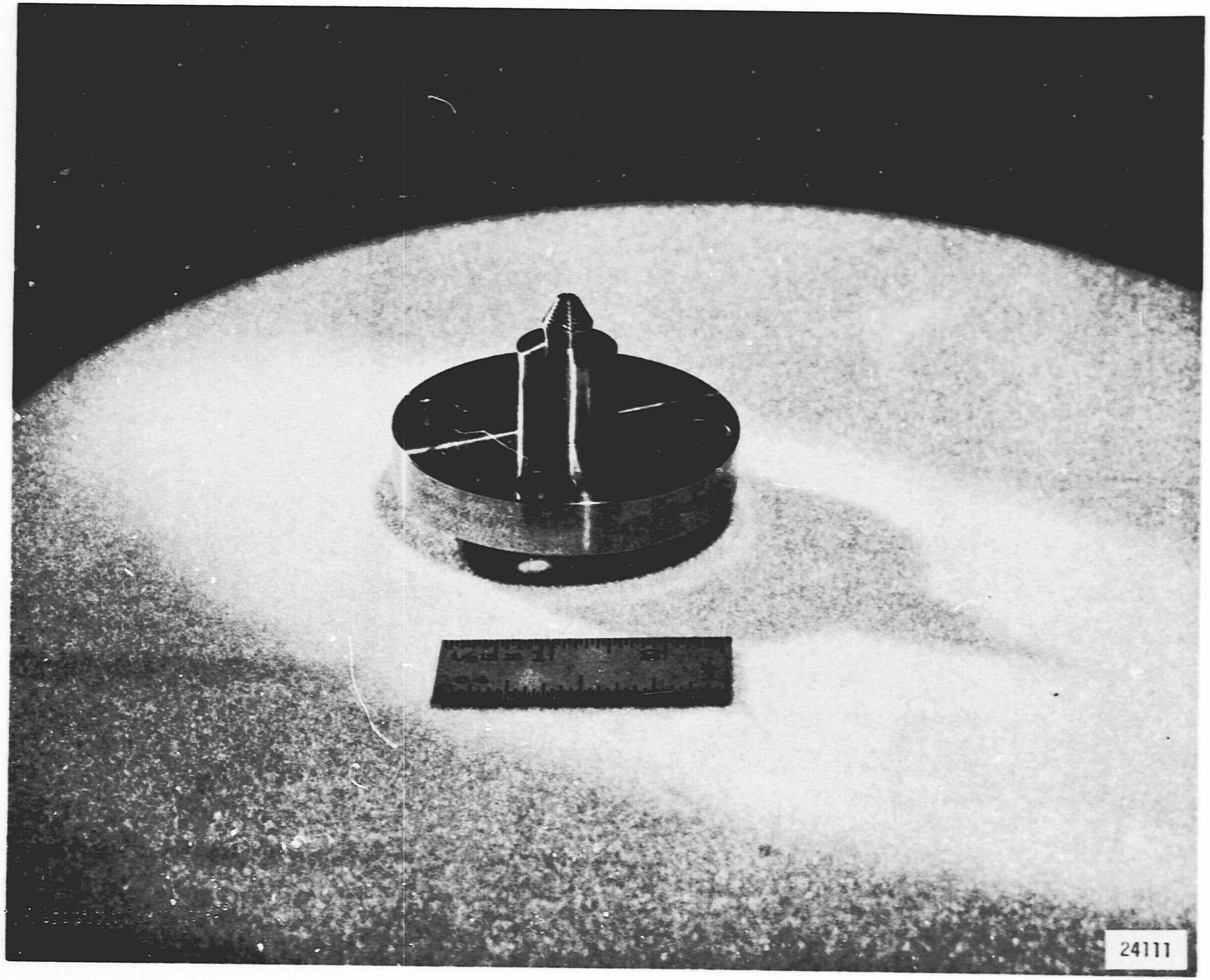

Fig. 4-2 - Test Shaft for Gyro Spin Axis Rotor with Spiral Grooved Conical Journal

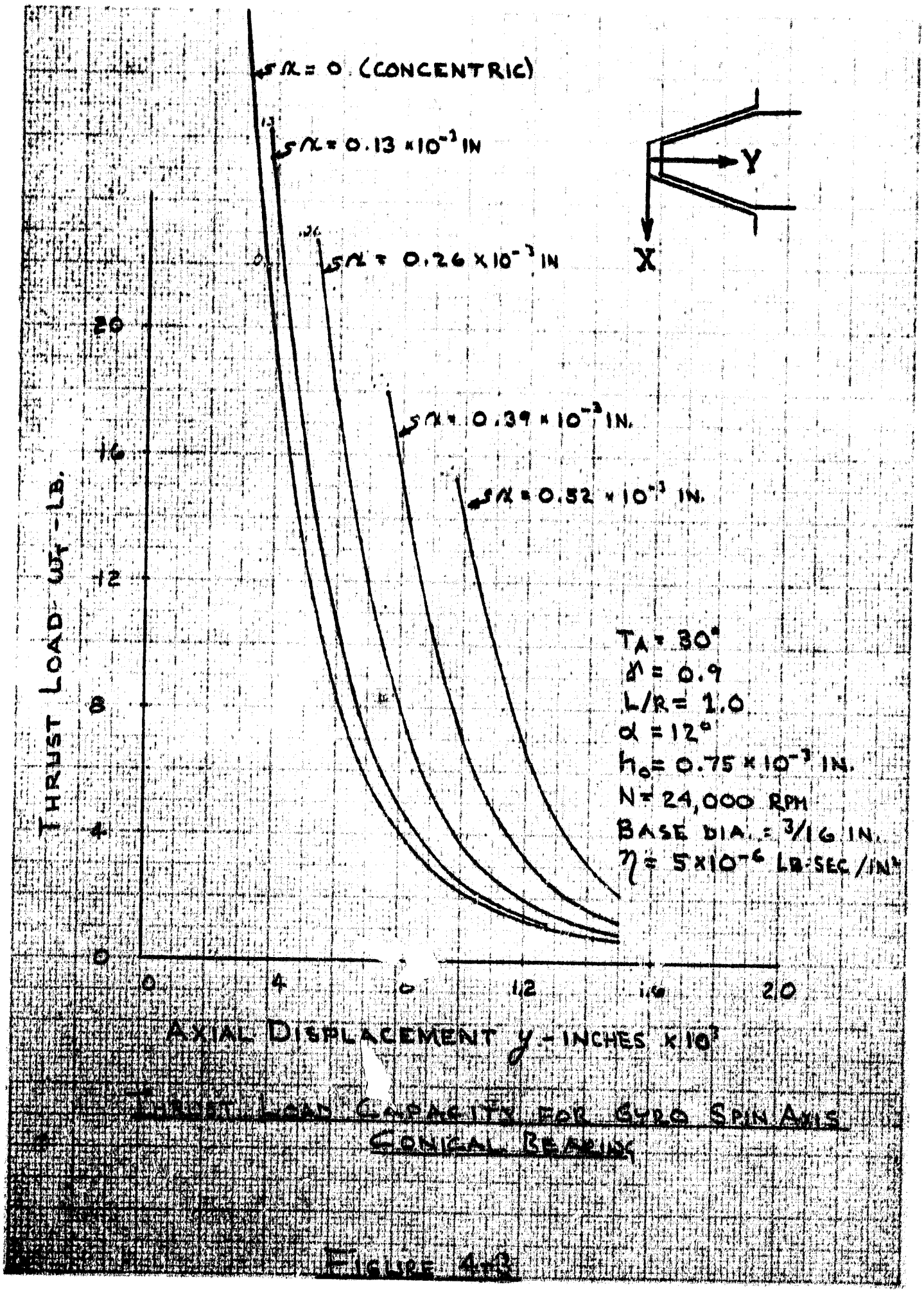

THRUST LOAD CAPACITY FOR GYRO SPIN AXIS CONICAL BEARING

FIGURE 4-3

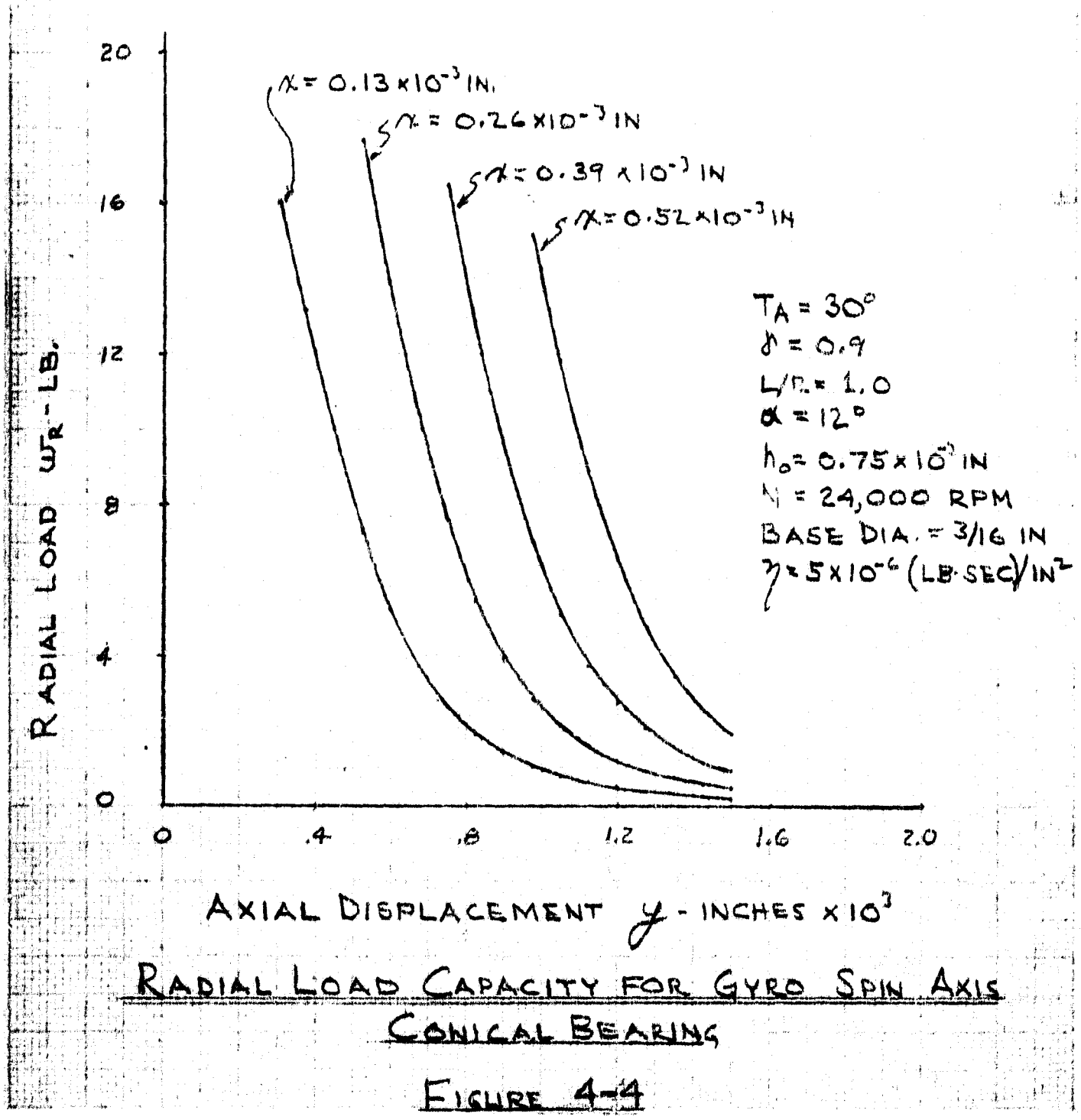

RADIAL LOAD CAPACITY FOR GYRO SPIN AXIS CONICAL BEARING

FIGURE 4-4

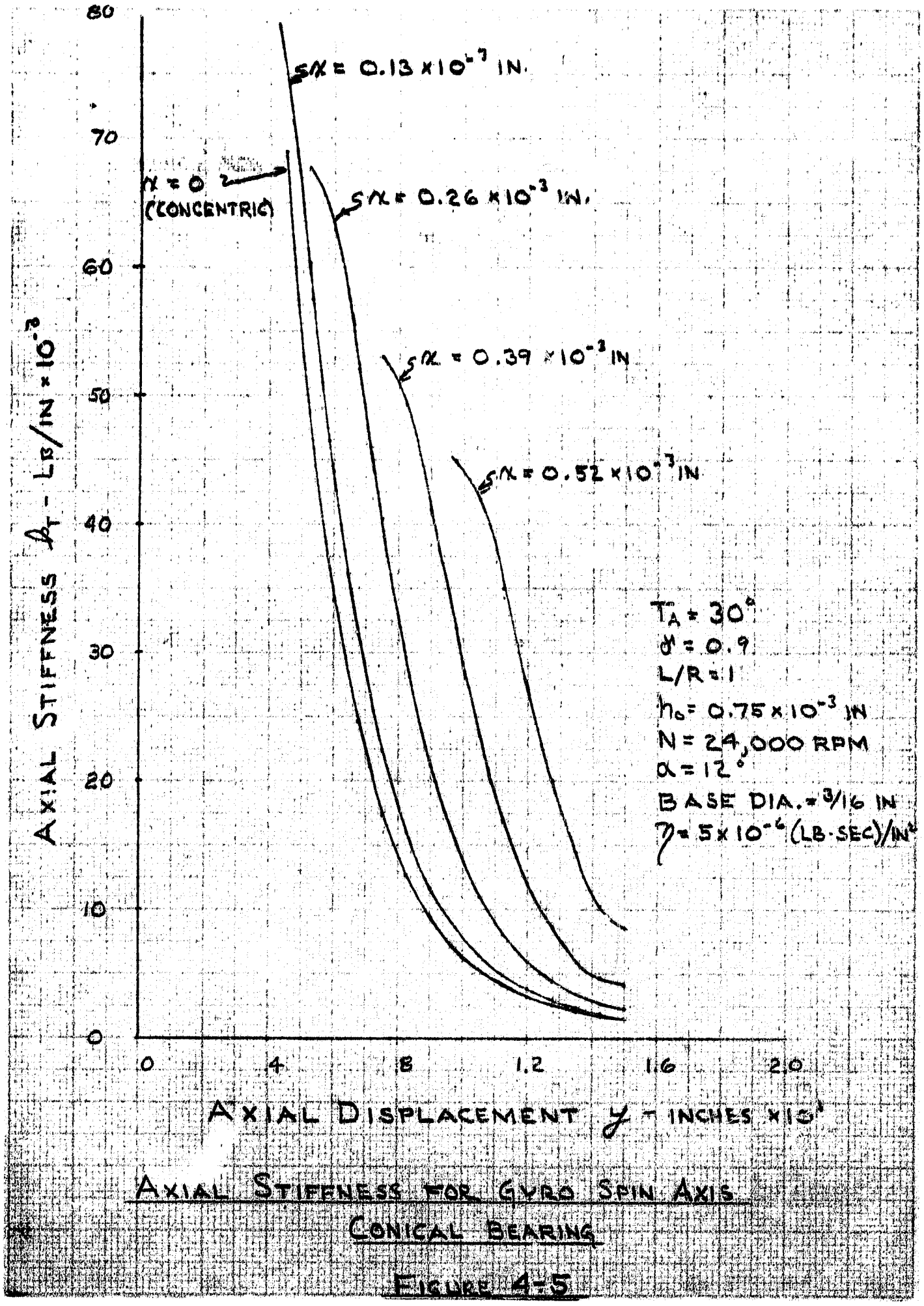

AXIAL STIFFNESS FOR GYRO SPIN AXIS
CONICAL BEARING

FIGURE 4-5

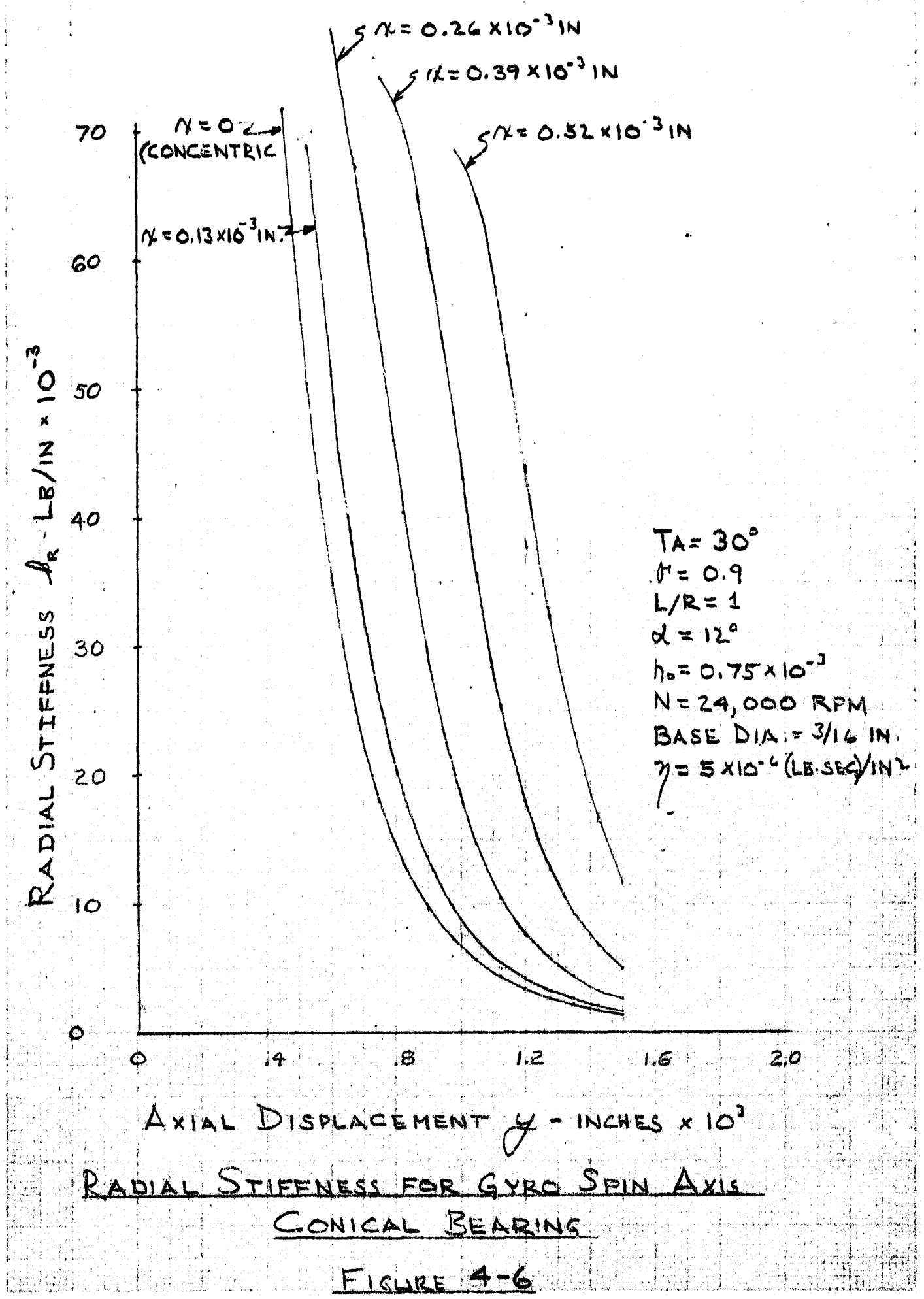

RADIAL STIFFNESS FOR GYRO SPIN AXIS CONICAL BEARING

FIGURE 4-6

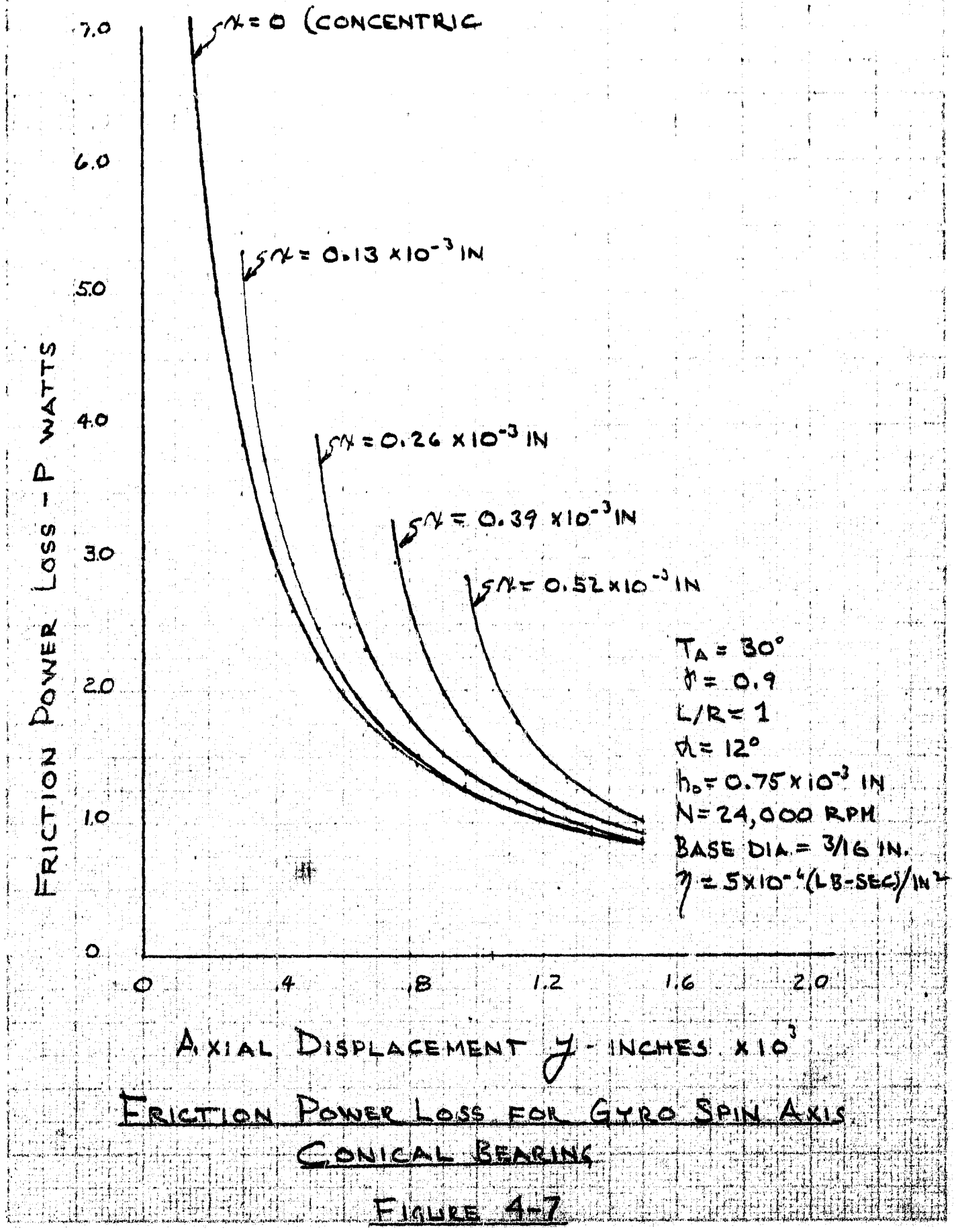

FRICTION POWER LOSS FOR GYRO SPIN AXIS CONICAL BEARING

FIGURE 4-7

Table 4.1

SCHEDULE OF OPERATING CONDITIONS FOR GYRO SPIN AXIS BEARINGS

Operating Mode	Bearing No.	Load		Power Loss watts	Compliance* micro in. per lb.		Minimum Clearance
		Thrust lb.	Radial lb.		Thrust	Radial	in. x 10^3
1g; Shaft Vertical	#1	4.1	0	1.48	70	68	0.40
	#2	5.2	0	1.64	51	50	0.36
1g; Shaft Horizontal	#1	4.7	0.3	1.58	60	59	0.36
	#2	4.7	0.3	1.58	60	59	0.36
6g; Shaft Vertical	#1	1.1	0	0.97	370	370	0.63
	#2	8.3	0	1.94	30	29	0.30
6g; Shaft Horizontal	#1	4.7	1.8	1.47	68	59	0.30
	#2	4.7	1.8	1.47	68	59	0.30

Initial Preload = 4.7 lb.

Shaft Weight = 0.6 lb.

*Approximate, see Section 5.3

4.4 Experimental Performance Data

Several experimental test runs were made to check the radial and axial loading methods, the torque read out system and the instrumentation. Spot checks of some of the experimental data indicated that the measured bearing friction was reasonably in agreement with the theoretical prediction for the concentric case.

Prior to the writing of this report, only one set of data was recorded that could be used to indicate bearing performance. This is given on Figure 4-8 which shows the relation between axial load and concentric clearance for the bearing described in Section 4.2. The agreement between experiment and theory is good.

A summary of experimental test experience is given in Section 8.4. This section describes some of the dynamical difficulties encountered in attempting to obtain more performance data.

EXPERIMENTAL MEASUREMENTS OF THRUST LOAD VS CONCENTRIC CLEARANCE FOR CONICAL SPIRAL GROOVE BEARING

ROTOR VERTICAL
TA = 30°
$\delta^* = 0.9$
L/R = 1
$\alpha = 12°$
$h_o = 0.75 \times 10^{-3}$ IN.
N = 24,000 RPM
BASE DIA. = 3/16 IN.
$\mu = 5 \times 10^{-8}$ LB-SEC/IN²
LUB. TYPE X-724-15 @ 120° F

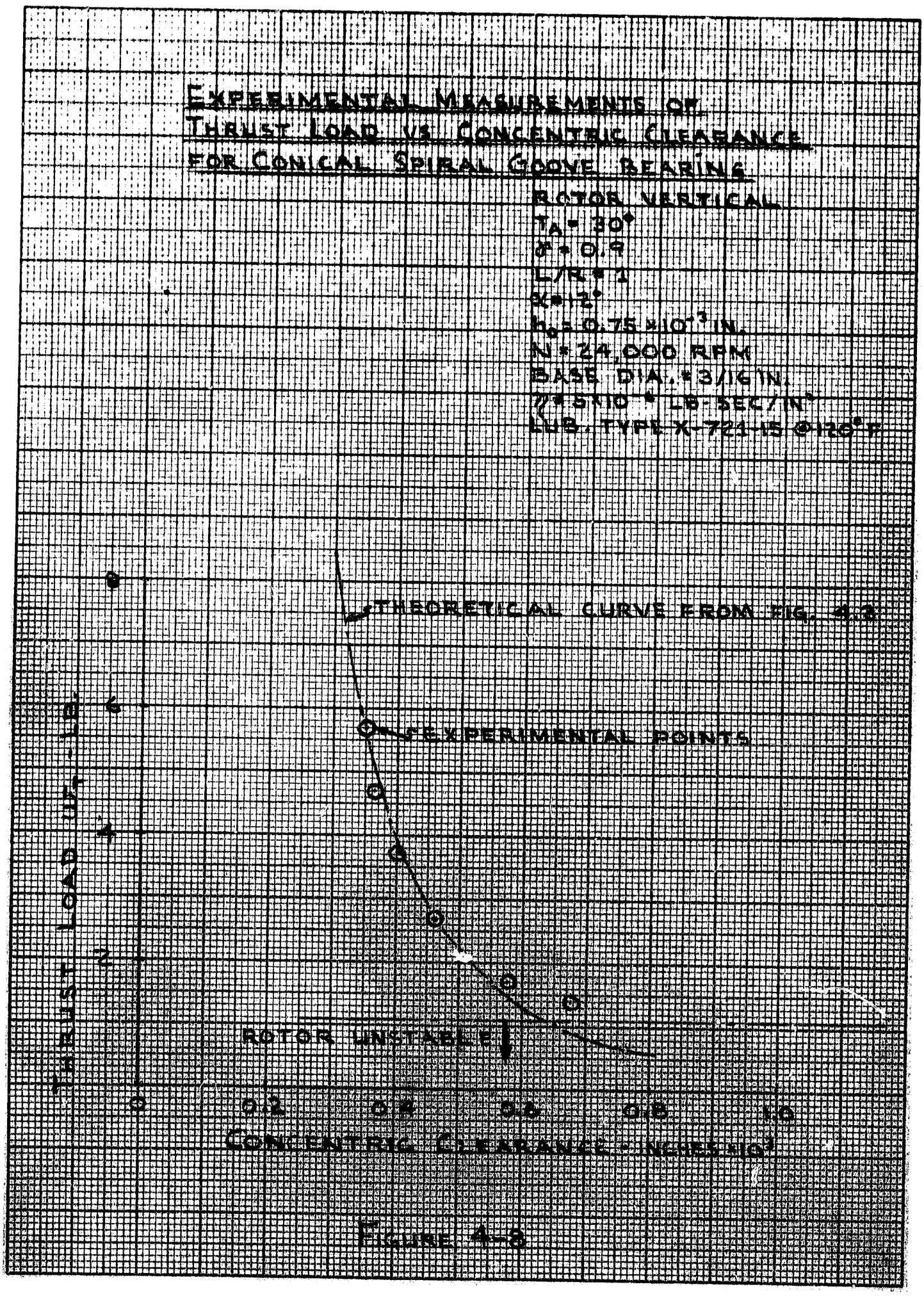

FIGURE 4-8

5. THEORETICAL ANALYSIS OF SPHERICAL AND CONICAL SPIRAL GROOVE BEARINGS

The present analysis of spherical and conical spiral groove bearings is based on the simplified model of the spiral pattern (Fig. 5-1) and the linear pressure distribution (Fig. 5-2) presented by Muijderman (Ref. 1). As a consequence of these assumptions the general expressions given in Ref. 1 for the pressure difference between two ends of the basic element, and also for frictional force, become directly applicable. For the case of no transverse flow (S = 0), these equations reduce to:

$$\frac{\Delta p h_o^2}{6\eta U_i d} = \frac{h_o^2}{h_2^2} \quad g_1(H,\gamma,\alpha) \tag{5.1}$$

and

$$\frac{|F|\ h_o}{\eta U_i d a_1} = \frac{h_o}{h_2}\ g_2(H,\gamma,\alpha) \tag{5.2}$$

where

$$g_1(H,\gamma,\alpha) = \frac{\gamma H^2 \cot\alpha\ (1 - H)(1 - H^3)}{(1 + \gamma H^3)(\gamma + H^3) + H^3 \cot^2\alpha\ (1 + \gamma)^2}$$

$$g_2(H,\gamma,\alpha) = \gamma + H + g_1(H,\gamma,\alpha)$$

a_1, a_2 = groove width, land width

$$H = \frac{h_2}{h_1} = \frac{\delta}{1 + \delta}$$

$\delta = h_2/h_o$

$\gamma = a_2/a_1$

U_1 = velocity of bearing surface

η = dynamic viscosity

α = angle between direction of U_1 and the groove tangent

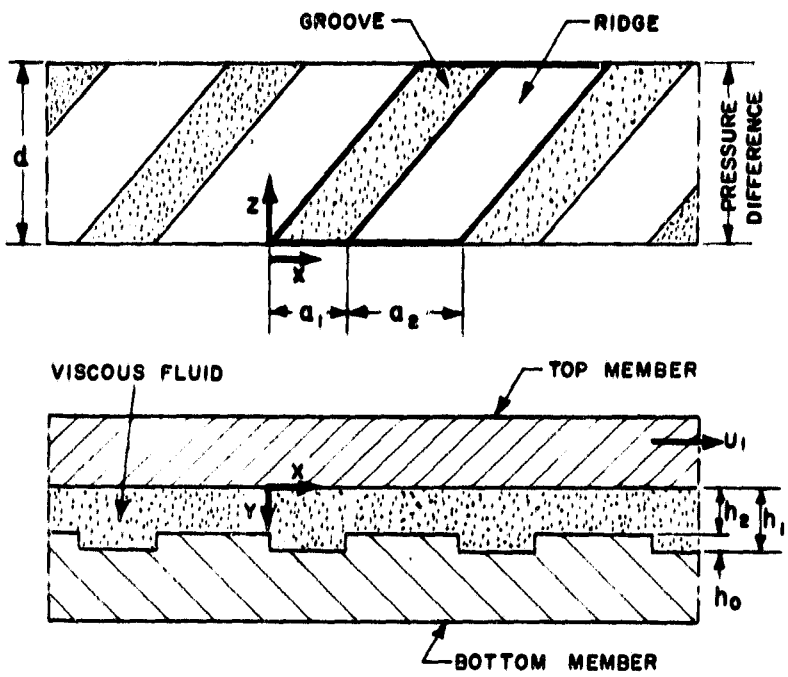

FIG. 5-1 MODEL OF PARALLEL SPIRAL GROOVE PATTERN

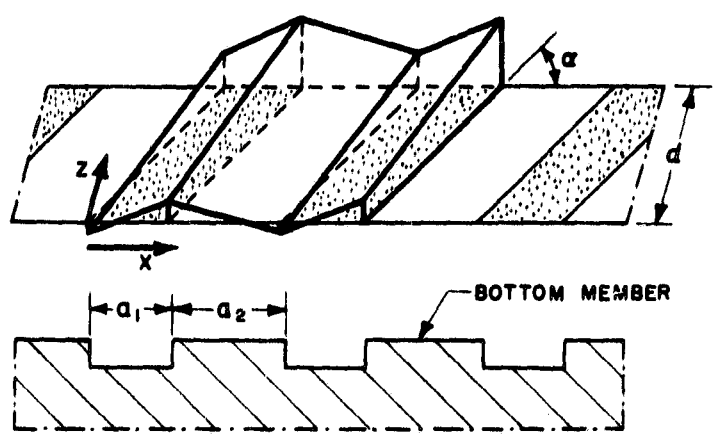

FIG. 5-2 LINEAR PRESSURE PROFILE

d = width of the basic element

Δp = pressure difference across the width of an element

$|F|$ = magnitude of frictional force over an element

Using (5.1) and (5.2) the load carrying capacity and the frictional moment can be computed with a simple integration. In the following, this integration is carried out separately for the spherical and conical bearings.

Two separate computer programs were written to implement the analyses. In spite of the rather large number of variables, these programs require little execution time to generate parametric performance studies.

5.1 Spherical Spiral Groove Bearings

Fig. 5-3 depicts the sphere and socket assemblage with a rectangular coordinate system (X,Y,Z) fixed at the center of the socket. In this coordinate system the position of the center of the sphere can be written as (X,Y,o) without loss of generality. The film thickness is found to be:

$$h_2 = C - X \sin\psi \cos\theta + Y \cos\psi \tag{5.3}$$

where ψ and θ are the two angles shown in Fig. 5-3 and C is the difference between the radius of the socket and that of the sphere.

For a spherical bearing the width of the element is:

$$d = R d\psi \tag{5.4}$$

and the velocity is:

$$U_1 = R\,\omega \sin\psi\,, \tag{5.5}$$

where R is the radius of the socket.

From (5.1) the pressure at any point on the bearing surface is found to be:

$$\frac{(p_a - p)\,h_o^2}{6\eta R^2 \omega} = \int_{\Psi}^{\Psi_2} \frac{h_o^2}{h_2^2}\, g_1(H,\gamma,\alpha) \sin\psi d\psi \tag{5.6}$$

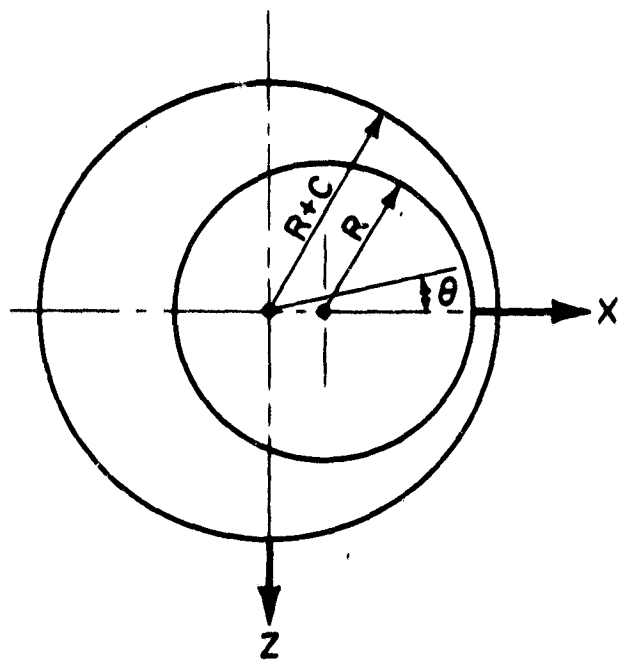

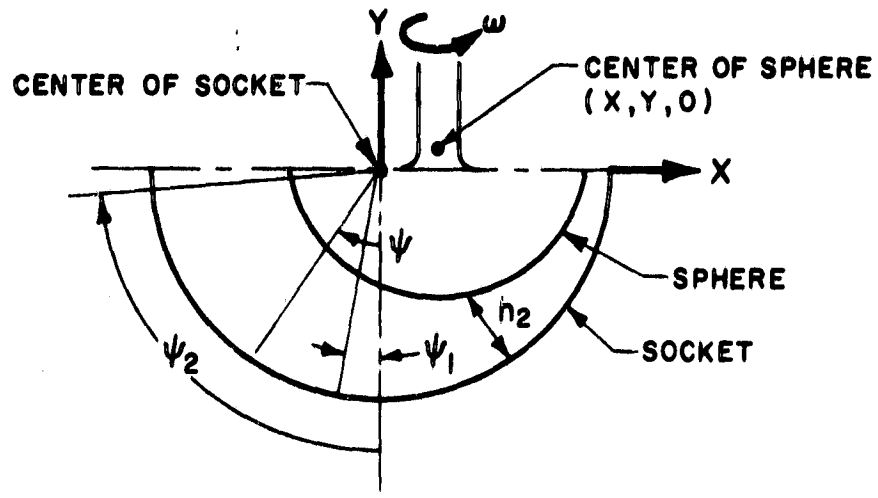

FIG. 5-3 SPHERICAL SPIRAL GROOVE BEARING COORDINATE

Here p_a is the pressure at $\psi = \psi_2$.

The thrust and radial load can be obtained by integrating (5,6) over the bearing surface. Thus,

$$W_T = \frac{w_t\, h_o^2}{6\eta\omega R^4} = \int_{\psi_1}^{\psi_2}\int_0^{2\pi} \frac{(p - p_a)h_o^2}{6\eta\omega R^2} \cos\psi \sin\psi \, d\theta \, d\psi$$

$$+ \frac{\sin^2\psi}{2} \int_0^{2\pi} \frac{(p_{\psi 1} - p_a)h_o^2}{6\eta\omega R^2} \, d\theta \qquad (5.7)$$

$$W_R = \frac{w_R\, h_o^2}{6\eta\omega R^4} = \int_{\psi_1}^{\psi_2}\int_0^{2\pi} \frac{(p - p_a)\, h_o^2}{6\eta\omega R^2} \sin^2\psi \, d\theta \, d\psi \qquad (5.8)$$

where $p_{\psi 1}$ is the pressure at $\psi = \psi_1$

Equations (5.7) and (5.8) give the load carrying capacity in the Y and X direction respectively. It should be noted that the second item in (5.7) is the contribution of the ungrooved portion of the bearing (i.e., $\psi_1 \neq 0$).

From (5.2) and (5.4) and (5.5) the friction moment is found to be

$$M = \frac{m_T\, h_o}{\eta\omega R^4} = \frac{1}{1+\gamma} \int_{\psi_1}^{\psi_2}\int_0^{2\pi} \frac{h_o}{h_2} g_2(H,\gamma,\alpha) \sin^3\psi \, d\theta \, d\psi \qquad (5.9)$$

5.2 Conical Spiral Groove Bearing

The conical bearing under consideration is shown in Fig. 5-4. For the sake of convenience, two coordinate systems are used. The X-Y system is fixed on the bearing, while the x-y system is attached to the conical rotor. Let h_i denote the distance between o and o' when the two surfaces are in contact and T_A be the half cone angle. The film thickness can be written as:

$$h_2 = h_i \sin T_A - X \cos T_A \cos\theta - Y \sin T_A \qquad (5.10)$$

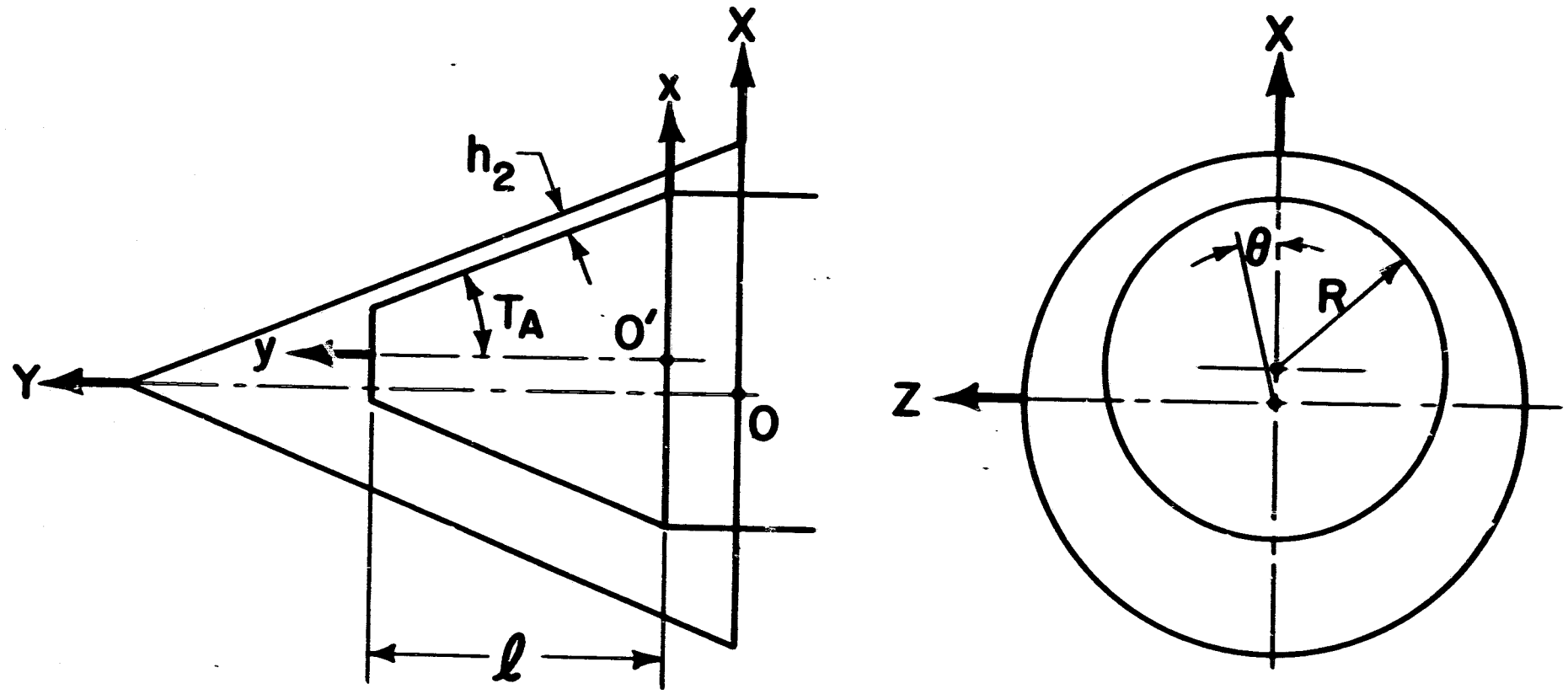

FIG. 5-4 CONICAL SPIRAL GROOVE BEARING COORDINATE

Since in this case:

$$d = \frac{dy}{\cos T_A} ,$$

and

$$U_1 = [R - y \tan T_A]\omega ,$$

where R is the radius of the cone at y = 0.

The pressure build-up is found to be:

$$\frac{(p - p_a)h_o^2}{6\eta\omega} = \frac{h_o^2}{h_2^2} \left[Ry - \frac{y^2}{2} \tan T_A\right] \frac{g_1(H,\gamma,\alpha)}{\cos T_A} \qquad (5.11)$$

It follows from (5.11) and (5.2) that the load capacity and frictional moments are:

$$W_T = \frac{w_t h_o^2}{6\eta R^4\omega} = \frac{1}{2} \frac{\tan T_A}{\cos T_A} \left[\frac{\ell}{R} - \frac{1}{2}\left(\frac{\ell}{R}\right)^2 \tan T_A\right]^2 \int_0^{2\pi} \frac{h_o^2}{h_2^2} g_1 \, d\theta$$
$$+ \left[\frac{\ell}{R} - \frac{1}{2}\left(\frac{\ell}{R}\right)^2 \tan T_A\right]\left[1 - \left(\frac{\ell}{R}\right) \tan T_A\right]^2 \int_0^{2\pi} g_1 \, d\theta \qquad (5.12)$$

$$W_R = \frac{w_R h_o^2}{6\eta R^4\omega} = \frac{1}{2} \tan t \left[\frac{\ell}{R} - \frac{1}{2}\left(\frac{\ell}{R}\right)^2 \tan T_A\right]^2 \int_0^{2\pi} \frac{h_o^2}{h_2^2} g_1 \, d\theta \qquad (5.13)$$

$$M = \frac{m h_o}{\eta R^4\omega} = \frac{1}{(1+\gamma)}\left(\frac{1}{\cos T_A}\right) \left[\frac{\ell}{R} - \frac{3}{2}\left(\frac{\ell}{R}\right)^2 \tan T_A + \left(\frac{\ell}{R}\right)^3 \tan^2 T_A\right.$$
$$\left. - \frac{1}{4}\left(\frac{\ell}{R}\right)^4 \tan^3 T_A\right] \int_o^{2\pi} \frac{h_o^2}{h_2^2} g_2 \, d\theta \qquad (5.14)$$

where ℓ is the length of the cone. Equation (5.12) and (5.13) give the load capacity in the axial and radial directions respectively. Eq. (5.14) gives the frictional moment of the bearing. It should be noted that the second term in (5.12) is the contribution from the end of the cone.

5.3 Remarks on the Analysis

As mentioned earlier, this analysis is based on the assumption of linear pressure distribution above the grooves and ridges. In Ref. 1 it is shown that this pressure profile satisfies the differential equation and the boundary condition along the edge of the grooves. But at the ends, the boundary condition of constant pressure cannot be satisfied. Thus, correction to the linear pressure distribution should be made to compensate for the end effect. In the present analysis the end effect was assumed to be negligibly small. Consequently Eq. (5.1) and (5.2) were used to calculate the load carrying capacity and the frictional moment.

A condition associated with the linear pressure distribution is that the film thickness must be constant over the entire surface. Strictly speaking, only the concentric cases in the spherical and conical bearings can be analyzed. However, it is felt that for cases where the film thickness deviates only slightly from the concentric cases useful information can still be obtained by using the linear profile. Thus, the expressions derived in Sections 5.1 and 5.2 are limited to small deviations from the concentric case.

Lastly, Equations (5.7) to (5.9) and (5.12) to (5.14 are valid only for an infinite number of grooves.

Because of these assumptions the results obtained here can only be regarded as a first approximation. They are used here to indicate feasibility and not as the final word in accurate design data. Experimental measurements have been made that indicate the dependability of the analysis for the uniform clearance case (Figures 4-8 and 7-2). More measurements are required to completely check the analysis.

6. A PARAMETRIC STUDY OF CONICAL BEARINGS

Film stiffness vs. the half-cone angle (T_A) is shown on Figure 6-1 for both the radial and axial directions. The two stiffnesses are seen to be equal when T_A is 29.3°. Note that T_A varies little from the optimum for a reduction in bearing clearance.

Groove angle (α) influence is given on Figure 6-2 for the relation between thrust load and friction torque. For low thrust loads the groove angle, α, should be large and for higher loads the groove angle should be small. Over limited load ranges, a small variation in α will not significantly affect the bearing friction torque. Thus, conventional machining processes may be used to cut the grooves, even though this results in a variation in α along the length of the cone.

The land to groove width ratio (γ) effect on thrust load, friction torque and film stiffness is given on Figures 6-3 and 6-4. Figure 6-3 shows for constant thrust load, γ should be minimized to reduce friction torque. On the other hand, for a given clearance, Figure 6-4 shows there is an optimum γ for both thrust load and stiffness. Moreover, γ is insensitive to moderate changes as film thickness. Thus it may be possible to cut grooves of constant width (resulting in a non-constant γ) without significantly affecting the bearing performance.

Groove depth (h_o) influence is shown Figures 6-5, 6-6 and 6-7 for thrust load, axial stiffness and power loss as a function of bearing separation. The major influence of h_o is on stiffness but for a significant load rang (corresponding to a relatively small change in film thickness) the bearing performance is insensitive to variations in h_o. Thus etching, which usually results in a rough groove bottom, is an acceptable technique for forming grooves in many applications.

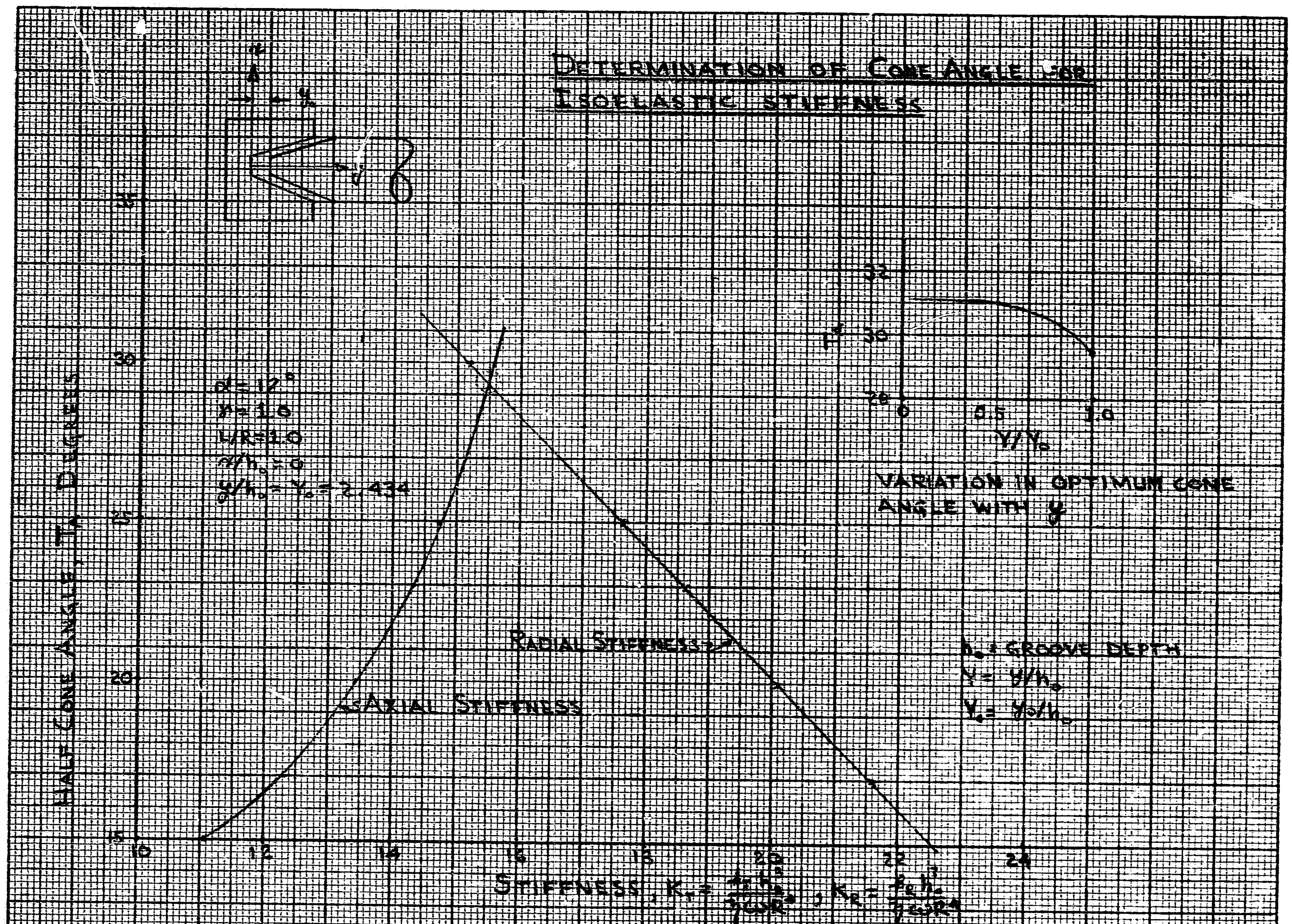
DETERMINATION OF CONE ANGLE FOR
ISOELASTIC STIFFNESS
HALF CONE ANGLE, TA DEGREES
15
20
25
30
35
10
12
14
16
18
20
22
24
α = 12°
λ = 1.0
L/R = 1.0
a/h₀ = 0
y/h₀ = Y₀ = 2.434
RADIAL STIFFNESS
AXIAL STIFFNESS
28
30
32
0
0.5
1.0
Y/Y₀
VARIATION IN OPTIMUM CONE
ANGLE WITH y
h₀ = GROOVE DEPTH
Y = y/h₀
Y₀ = y₀/h₀
STIFFNESS, K_T = , K_R =

FIGURE 6-1

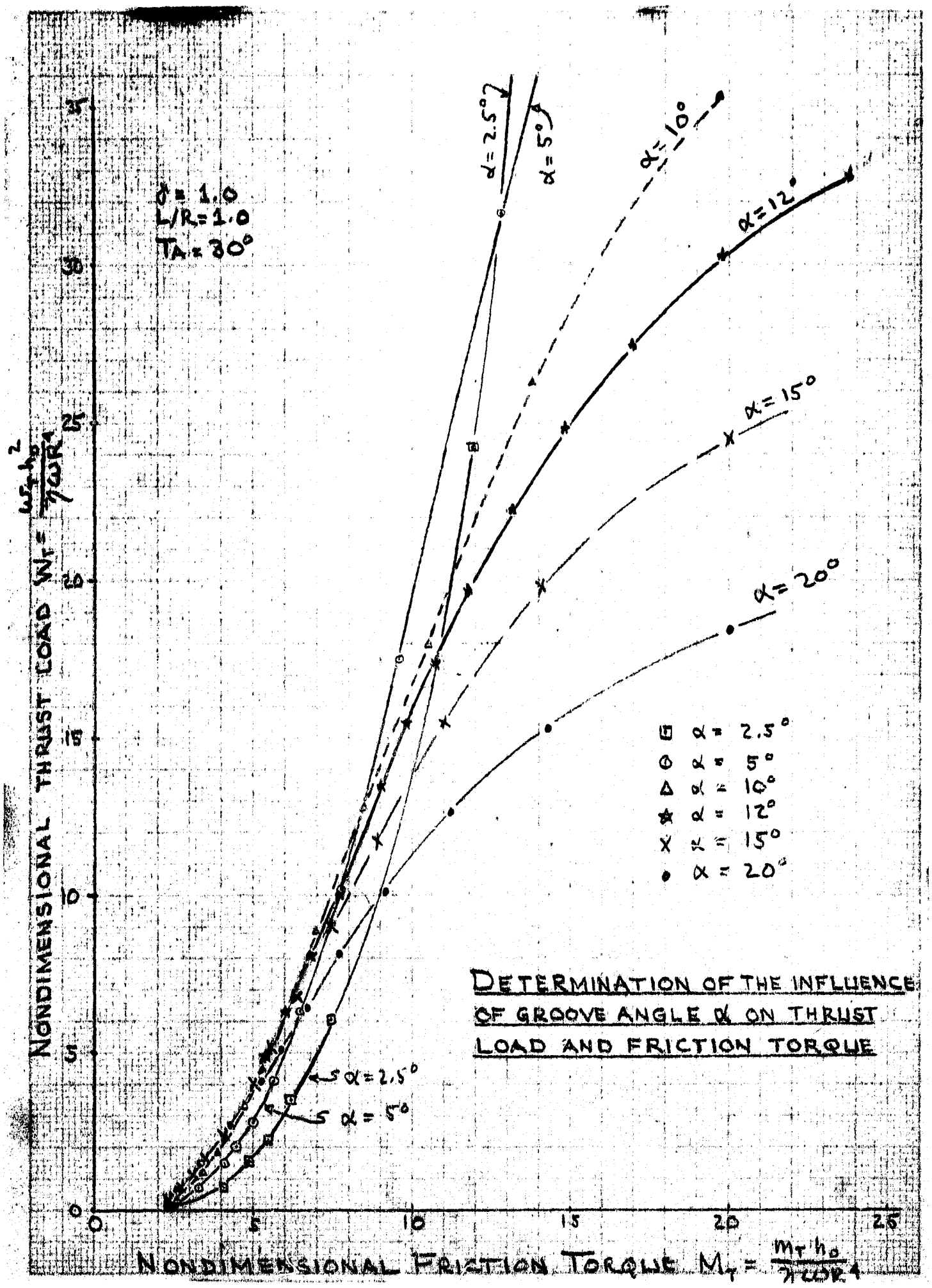

DETERMINATION OF THE INFLUENCE OF GROOVE ANGLE α ON THRUST LOAD AND FRICTION TORQUE

Fig. 6-2

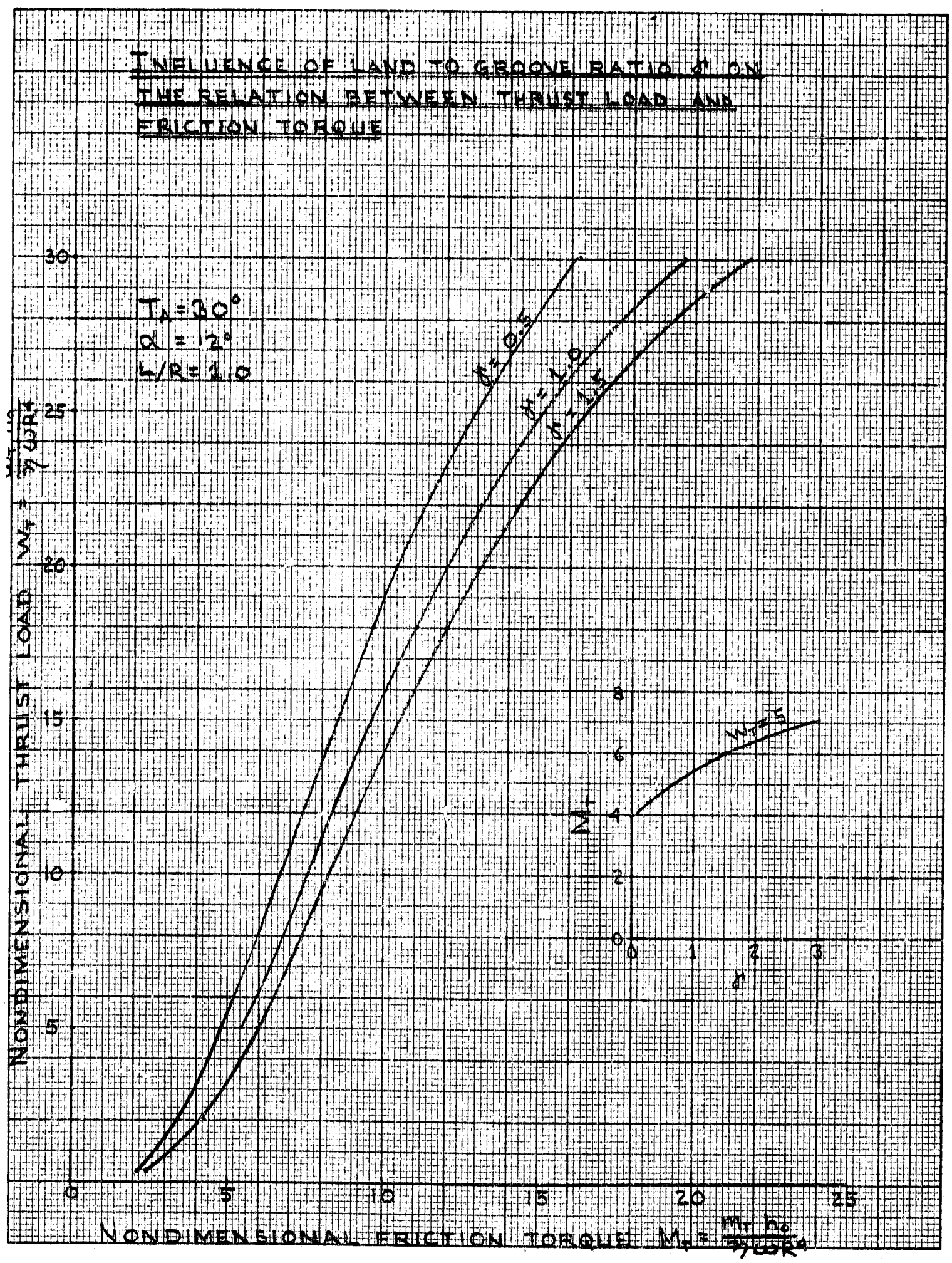
INFLUENCE OF LAND TO GROOVE RATIO δ* ON THE RELATION BETWEEN THRUST LOAD AND FRICTION TORQUE
$T_1 = 30°$
$\alpha = 12°$
$L/R = 1.0$
$\delta^* = 0.5$
$\delta^* = 1.0$
$\delta^* = 1.5$
$W_T = 5$
LOAD $W_T = \frac{W}{\pi \omega R^4}$
NONDIMENSIONAL THRUST
NONDIMENSIONAL FRICTION TORQUE $M_T = \frac{m_T h_0}{\pi \omega R^4}$
Σ^*
δ^*

Fig. 6-3

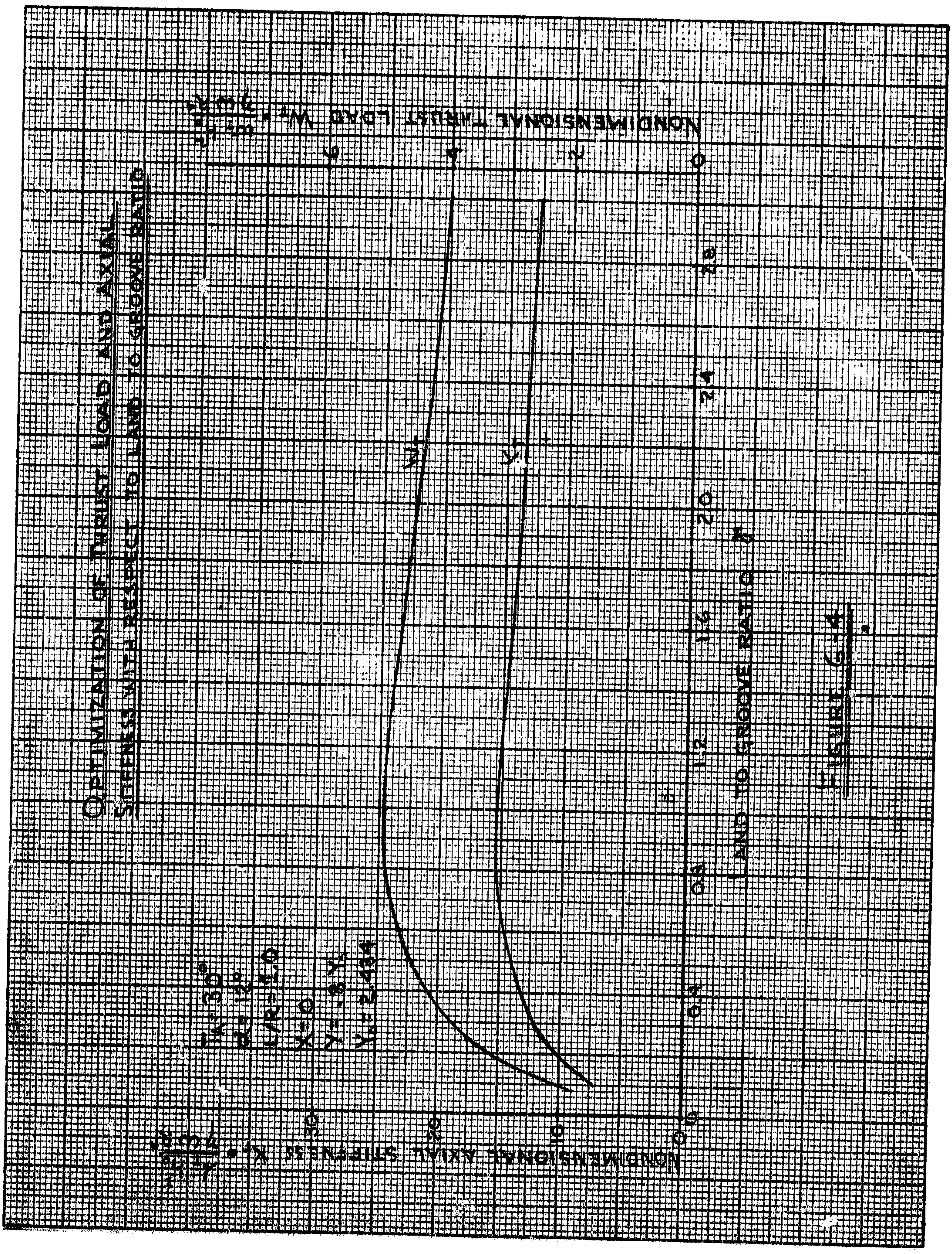

OPTIMIZATION OF THRUST LOAD AND AXIAL STIFFNESS WITH RESPECT TO LAND TO GROOVE RATIO

FIGURE 6-4

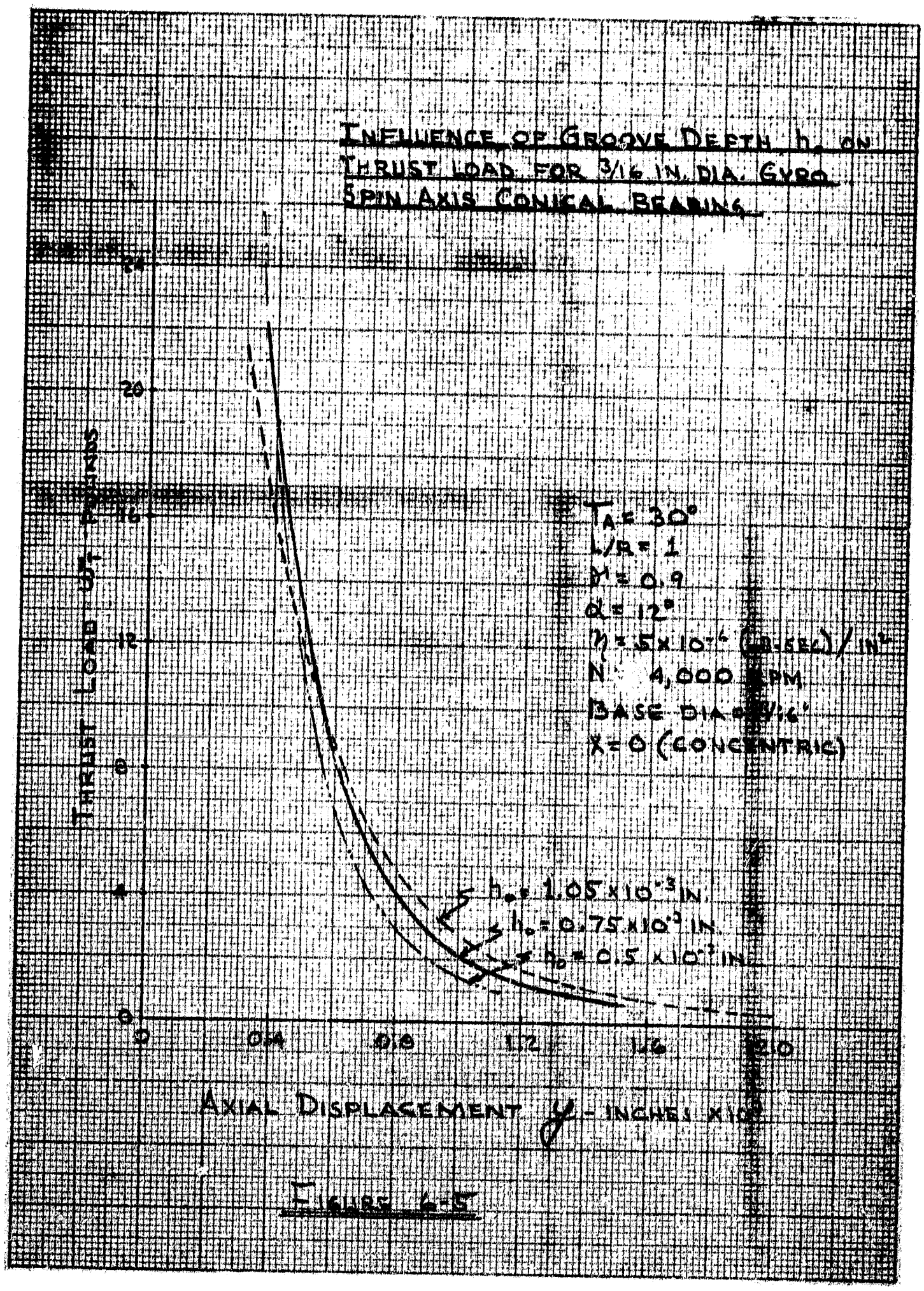
INFLUENCE OF GROOVE DEPTH h_o ON THRUST LOAD FOR 3/16 IN. DIA. GYRO 5 PIN AXIS CONICAL BEARING
THRUST LOAD - LBS
AXIAL DISPLACEMENT δ - INCHES X10^{-3}
T_A = 30°
L/R = 1
γ = 0.9
α = 12°
η = 5 X 10^{-6} (LB-SEC) / IN^2
N = 4,000 RPM
BASE DIA = 3/16"
X = 0 (CONCENTRIC)
h_o = 1.05 X 10^{-3} IN.
h_o = 0.75 X 10^{-3} IN.
h_o = 0.5 X 10^{-3} IN.
0
4
8
12
16
20
0.4
0.8
1.2
1.6
2.0

FIGURE 6-5

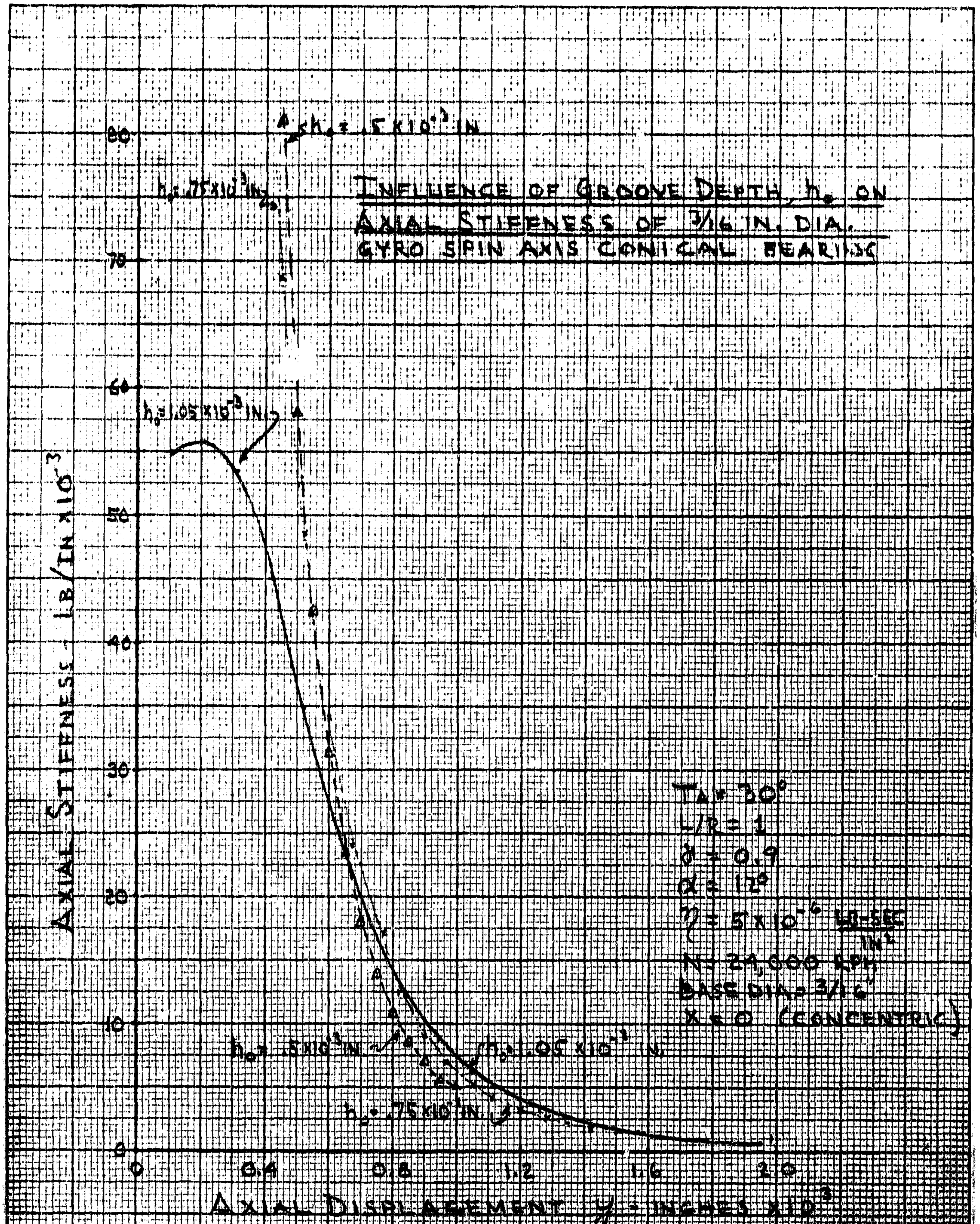
INFLUENCE OF GROOVE DEPTH, h_o ON
AXIAL STIFFNESS OF 3/16 IN. DIA.
GYRO SPIN AXIS CONICAL BEARING
$h_o = .5 \times 10^{-3}$ IN
$h_o = .75 \times 10^{-3}$ IN
$h_o = 1.05 \times 10^{-3}$ IN
TA = 30°
L/R = 1
γ = 0.9
α = 12°
$\eta = 5 \times 10^{-6}$ LB-SEC/IN²
N = 24,000 RPM
BASE DIA. = 3/16"
X = 0 (CONCENTRIC)
AXIAL STIFFNESS - LB/IN $\times 10^{-3}$
AXIAL DISPLACEMENT y - INCHES $\times 10^{-3}$
0
10
20
30
40
50
60
70
80
0.4
0.8
1.2
1.6
2.0
FIGURE 6.6

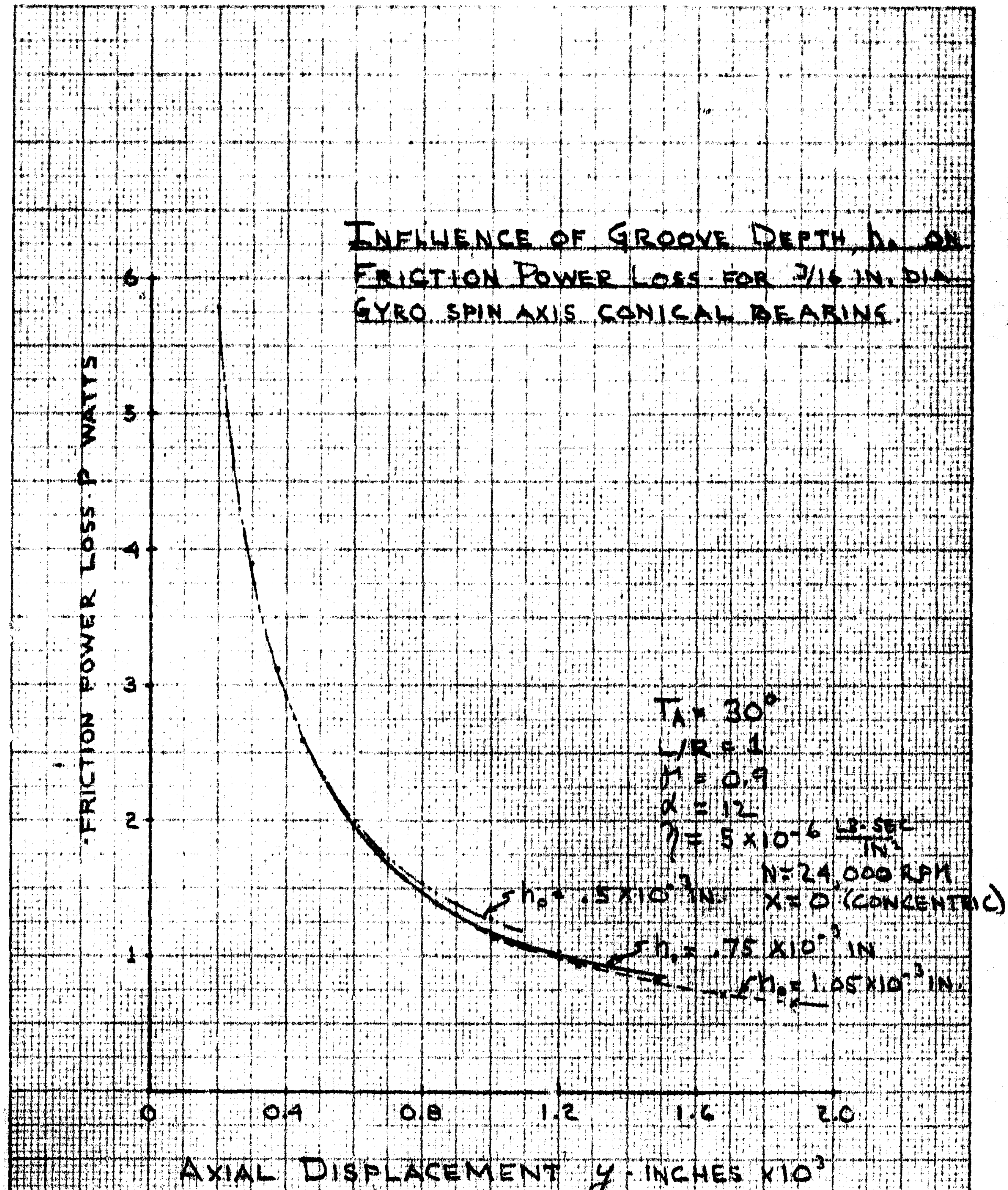
INFLUENCE OF GROOVE DEPTH, h₀ ON FRICTION POWER LOSS FOR 3/16 IN. DIA. GYRO SPIN AXIS CONICAL BEARING
FRICTION POWER LOSS P WATTS
1
2
3
4
5
6
0
0.4
0.8
1.2
1.6
2.0
AXIAL DISPLACEMENT y - INCHES X10³
T_A = 30°
L/R = 1
μ = 0.9
α = 12
η = 5 x 10⁻⁶ LB·SEC/IN²
N = 24,000 RPM
X = 0 (CONCENTRIC)
h₀ = .5 X10⁻³ IN.
h₀ = .75 X10⁻³ IN
h₀ = 1.05 X10⁻³ IN.

FIGURE 6.7

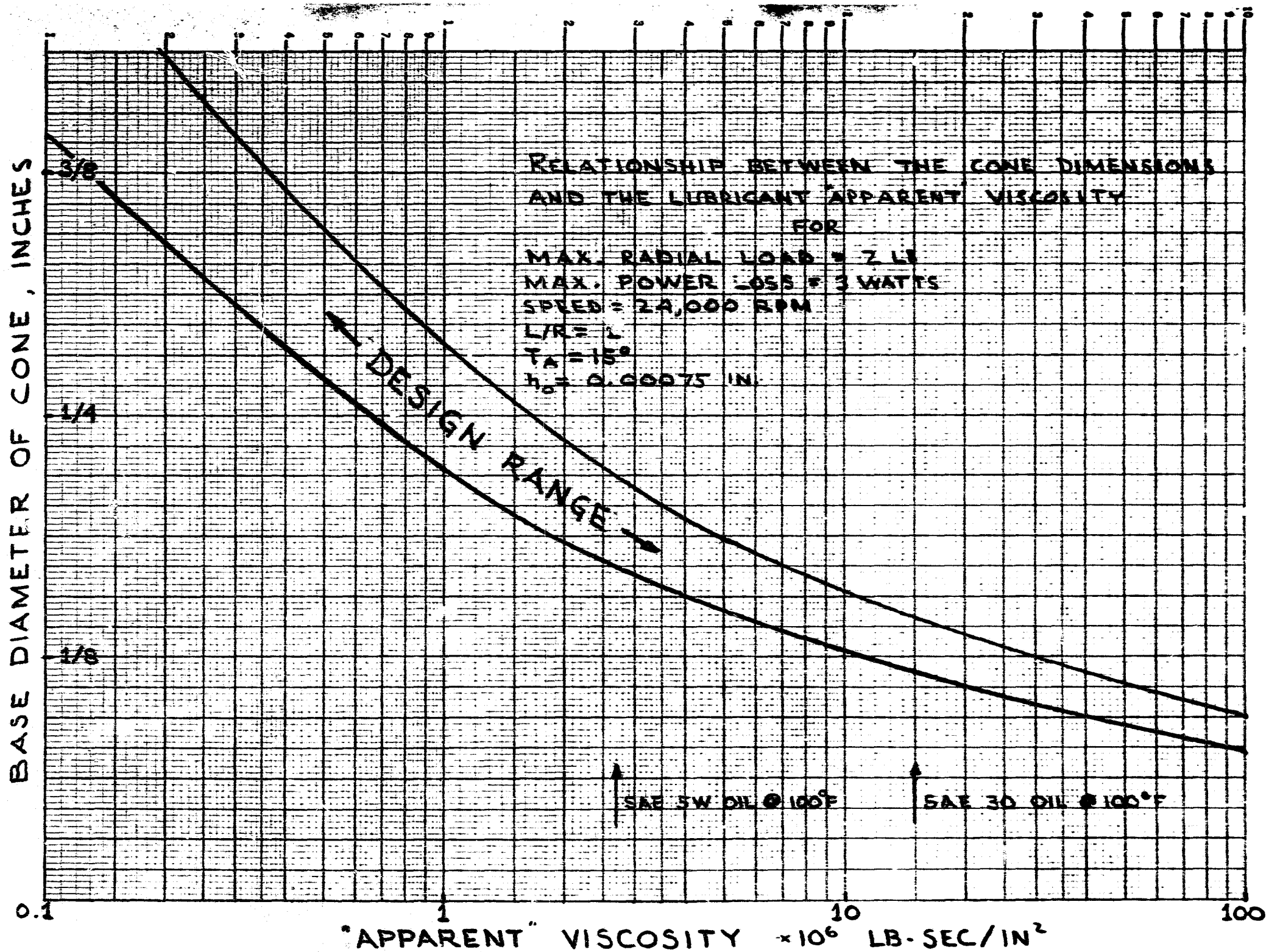
RELATIONSHIP BETWEEN THE CONE DIMENSIONS AND THE LUBRICANT "APPARENT" VISCOSITY FOR
MAX. RADIAL LOAD = 2 LB
MAX. POWER LOSS = 3 WATTS
SPEED = 24,000 RPM
L/R = 1
T_A = 15°
h_o = 0.00075 IN.
DESIGN RANGE
SAE 5W OIL @ 100°F
SAE 30 OIL @ 100°F
BASE DIAMETER OF CONE, INCHES
3/8
1/4
1/8
0.1
1
10
100
"APPARENT" VISCOSITY ×10⁶ LB-SEC/IN²

Fig. 6-8

For given parameters and cone proportions, Figure 6-8 gives an approximate relation between the "apparent" viscosity of the lubricant and the cone base diameter. In the analysis it is assumed that the bearing film strain rate is high enough so that the viscosity of the non-Newtonian grease is adequately represented by the viscosity of its base oil. The information provided by Figure 6-8 led to the selection of a 3/16 in. base diameter cone in order to satisfy the specifications of Section 4.1.

The data given in this section was used to design the bearing described in Section 4. Even more important, these data were used to specify *design tolerances*.

7. EXPERIMENTS WITH SINGLE BEARING TEST RIG

7.1 Description of Rig

The single bearing test rig (SBTR) is an FIRL experimental facility built to investigate the properties of grease lubricated spiral groove bearings. This rig was used to partially validate the analysis described in Section 5 and to aid in selecting optimum properties for the gyro grease lubricant.

Figure 7-1 shows a sketch of the SBTR. Basically, the rig consists of a belt driven rotor, a load piston, a spherical aligning surface and a torque disc. The piston passes through a labyrinth sealed (not shown) pressure chamber and its axial motion is guided by a hydrostatic air lubricated journal bearing. Axial load is applied by pressurizing the piston cylinder. The test bearing is fixed to the torque disc which is also supported on a hydrostatic air bearing. Bearing friction torque is computed from measurements of the force required to restrain the torque disc from rotation. Radial load is applied to the bearing by a wire, pulley and "dead weight" platform arrangement. The journal for the test bearing is machined on the end of a spindle which is threaded into the belt driven rotor. Spindle speed (up to 10,000 rpm) is controlled by mounting various pulley combinations on the motor and rotor shafts.

7.2 Partial Validations of the Analyses

In order to estimate the validity of the conical bearing analysis given in Section 5, an experimental test was conducted to determine the relation between thrust load and frictional torque. A conical bearing (see sketch on Figure 7-2) was machined taking no precautions to maintain a constant groove angle, α, land to groove ratio, γ, or a precise groove depth, h_o. In order to avoid the analytical complication of a non-Newtonian fluid, a Newtonian oil with well known properties was used

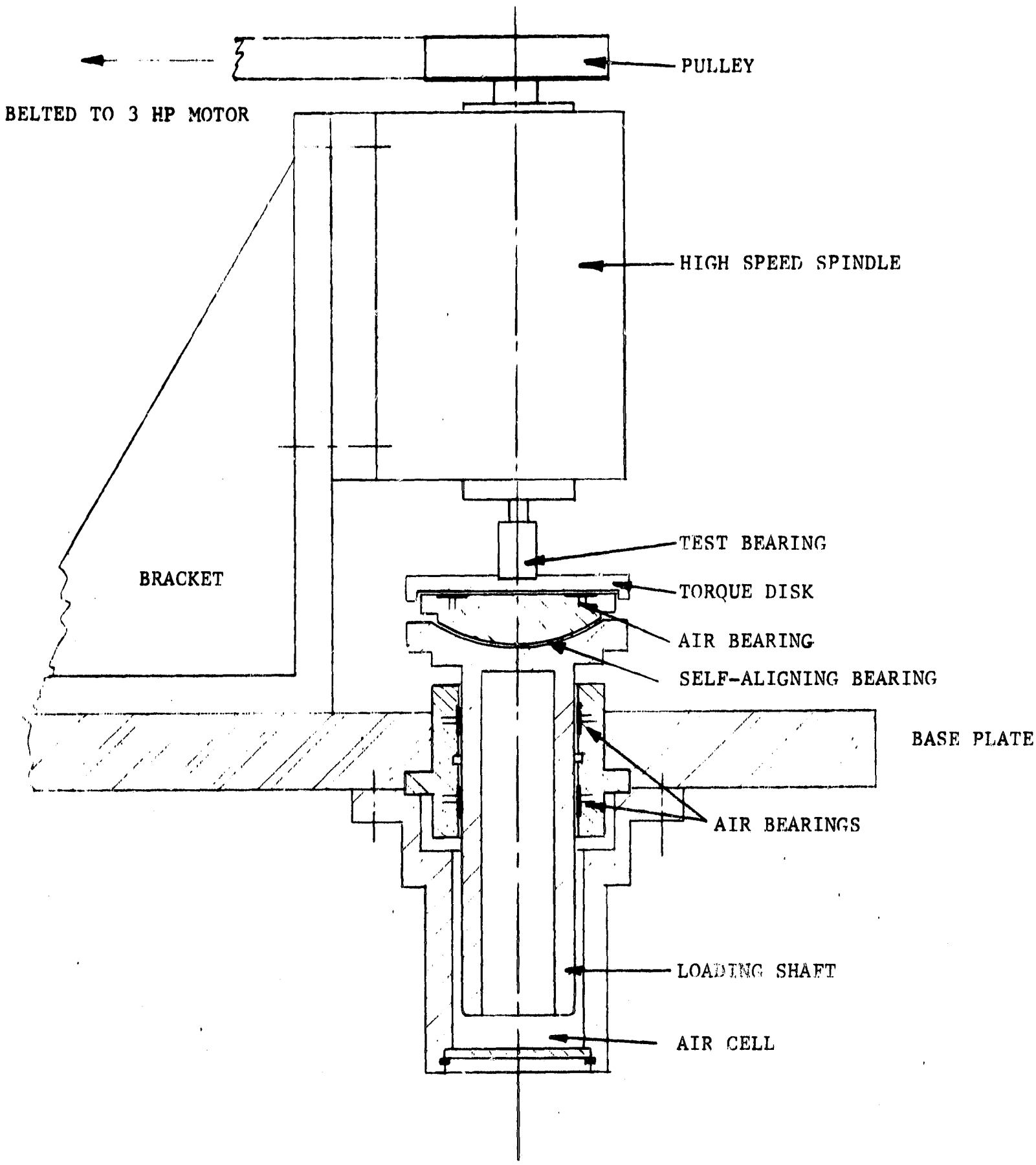

FIGURE 7-1 SINGLE BEARING TEST RIG

COMPARISON OF EXPERIMENTAL DATA TAKEN ON FIRL SINGLE BEARING TEST RIG WITH SPIRAL GROOVE CONICAL BEARING THEORETICAL ANALYSIS

$T_a = 15^\circ$
$L/R = 1.5$
$X = 0$ (CONCENTRIC)

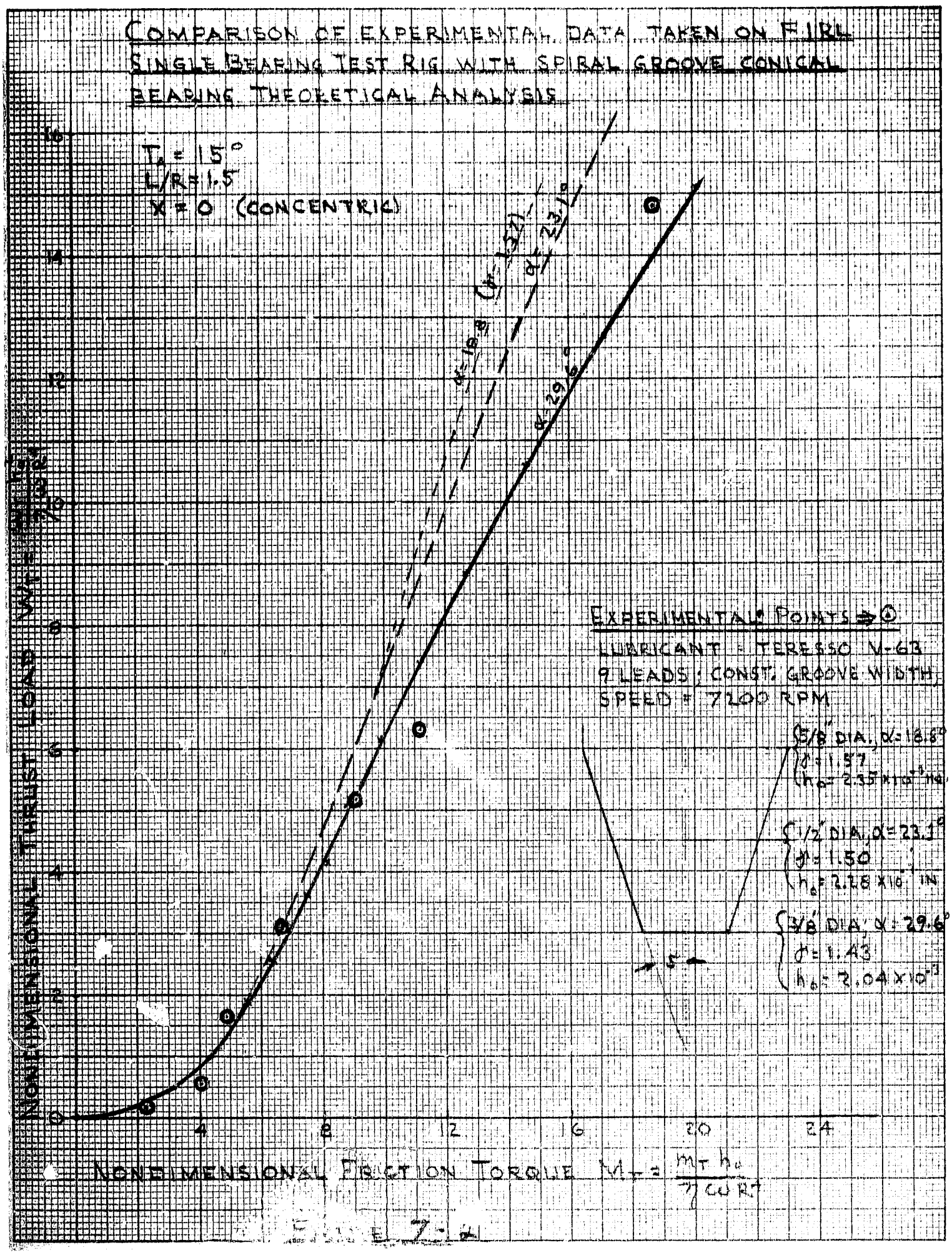

FIG. 7-2

as the lubricant. Theoretical curves corresponding to the groove geometry at the base, mid and end planes were computed and plotted on Figure 7-2. The dark circles on this figure are the experimental obtain points. Note that the experimental data agrees well with the analysis. Also, there is an indication that the groove geometry at the end of the cone (the high pressure section) essentially dictates the bearing performance. Additional confirmation of the analysis (relating clearance and thrust load) was previously discussed in Section 4.4.

7.3 Lubricant Selection

Figure 7-3 shows the test set-up of the SBTR for lubricant screening. The geometry of the cone used for all screening tests is that shown on Figure 7-2. Figure 7-3 shows the bearing with a grease fitting extending to the left and three thermocouples wires on the right leading to a continuous, multi-channel temperature recorder. The air bearing supported torque disc has two rods attached horizontally, one of which bears against a strain gauge force transducer and restrains the rotation of the disc. Thus, the test bearing shear torque is monitored by the strain gauge and plotted by the pen recorder placed at the left of the bed plate.

Two of the thermocouples are imbedded in the skin of the bearing. These are referred to as T_1 and T_2. The third thermocouple, T_3 is located in the lubricant cavity below the transcated end of the cone.

Figure 7-4 and 7-5 show typical test results for a "well behaved" and a "poorly behaved" grease. Table 7-1 shows a comparison among some of the tested grease samples. These test results do not identify the "best" or "only" lubricant for the present design problem. There are many potentially successful greases that were not investigated due to the usual time and money limitations imposed by the very nature of a feasibility study. Nevertheless, based on testing experience to date, the grease lubricant for the design given in Section 4.2 should have the following properties:

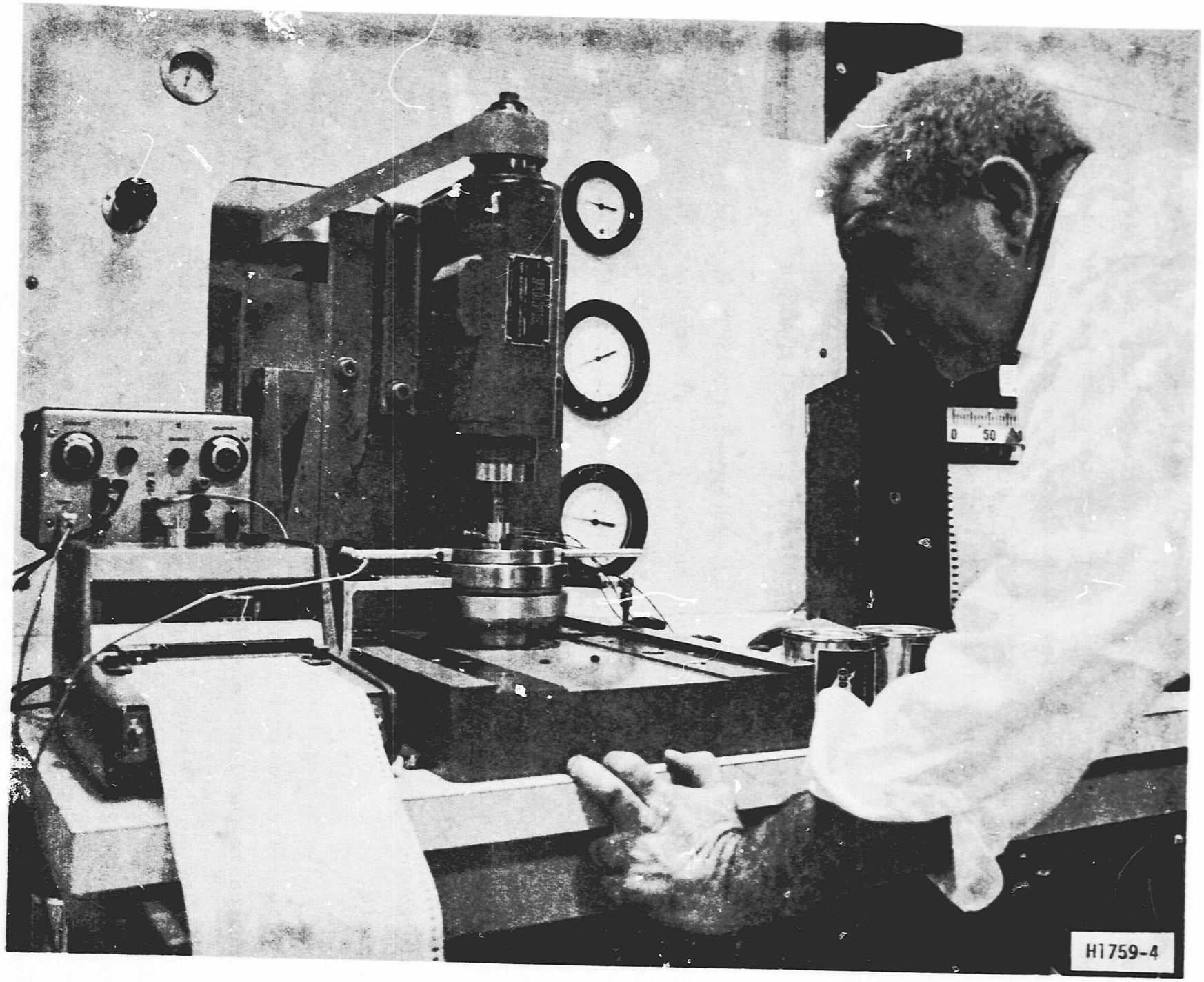

Fig. 7-3 - FIRL Single Bearing Test Rig Set-up for Lubricant Study

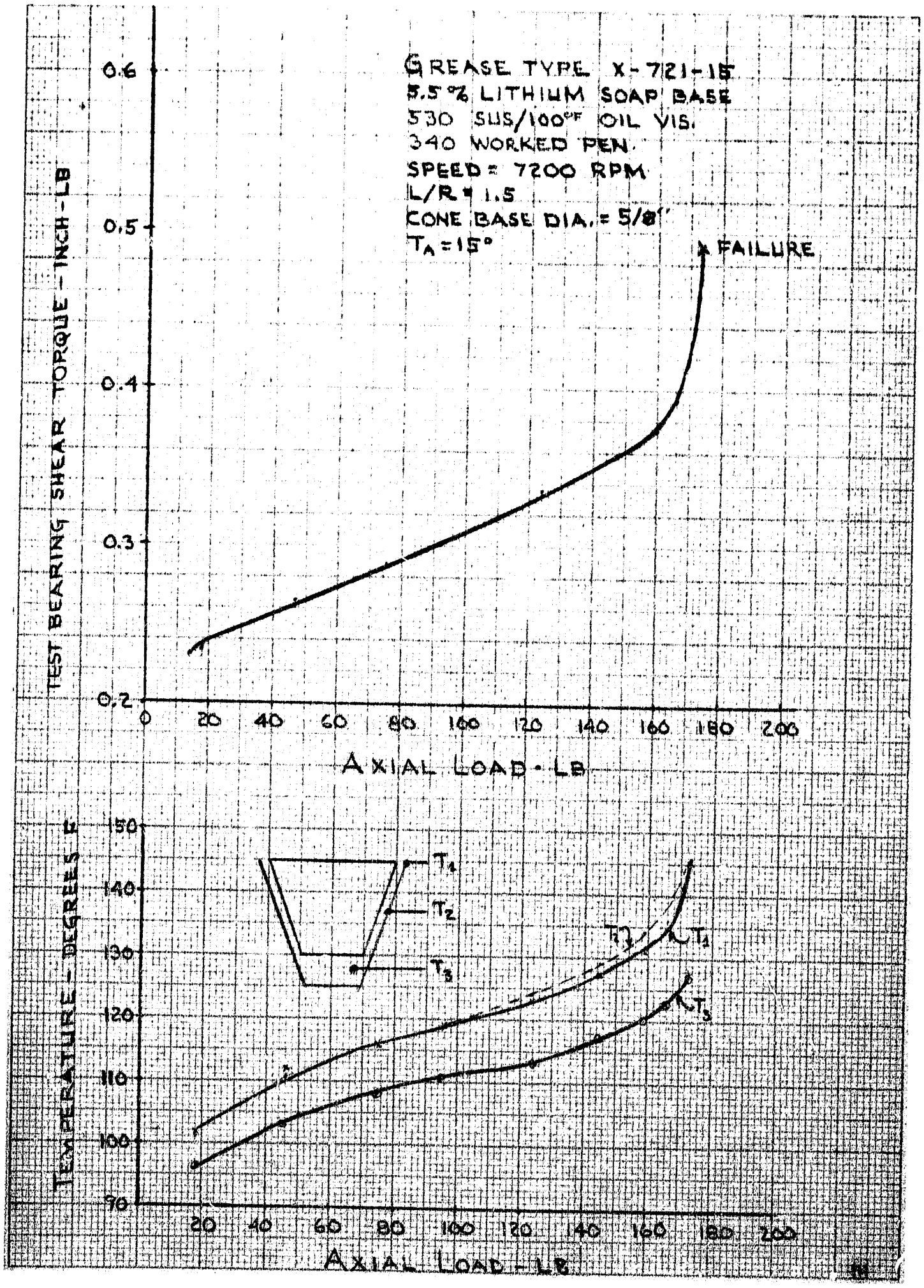
GREASE TYPE X-721-15
5.5% LITHIUM SOAP BASE
530 SUS/100°F OIL VIS.
340 WORKED PEN.
SPEED = 7200 RPM
L/R = 1.5
CONE BASE DIA. = 5/8"
T_A = 15°
FAILURE
TEST BEARING SHEAR TORQUE - INCH-LB
0.6
0.5
0.4
0.3
0.2
0
20
40
60
80
100
120
140
160
180
200
AXIAL LOAD - LB
TEMPERATURE - DEGREES F
150
140
130
120
110
100
90
T_1
T_2
T_3
AXIAL LOAD - LB

Fig. 7-4

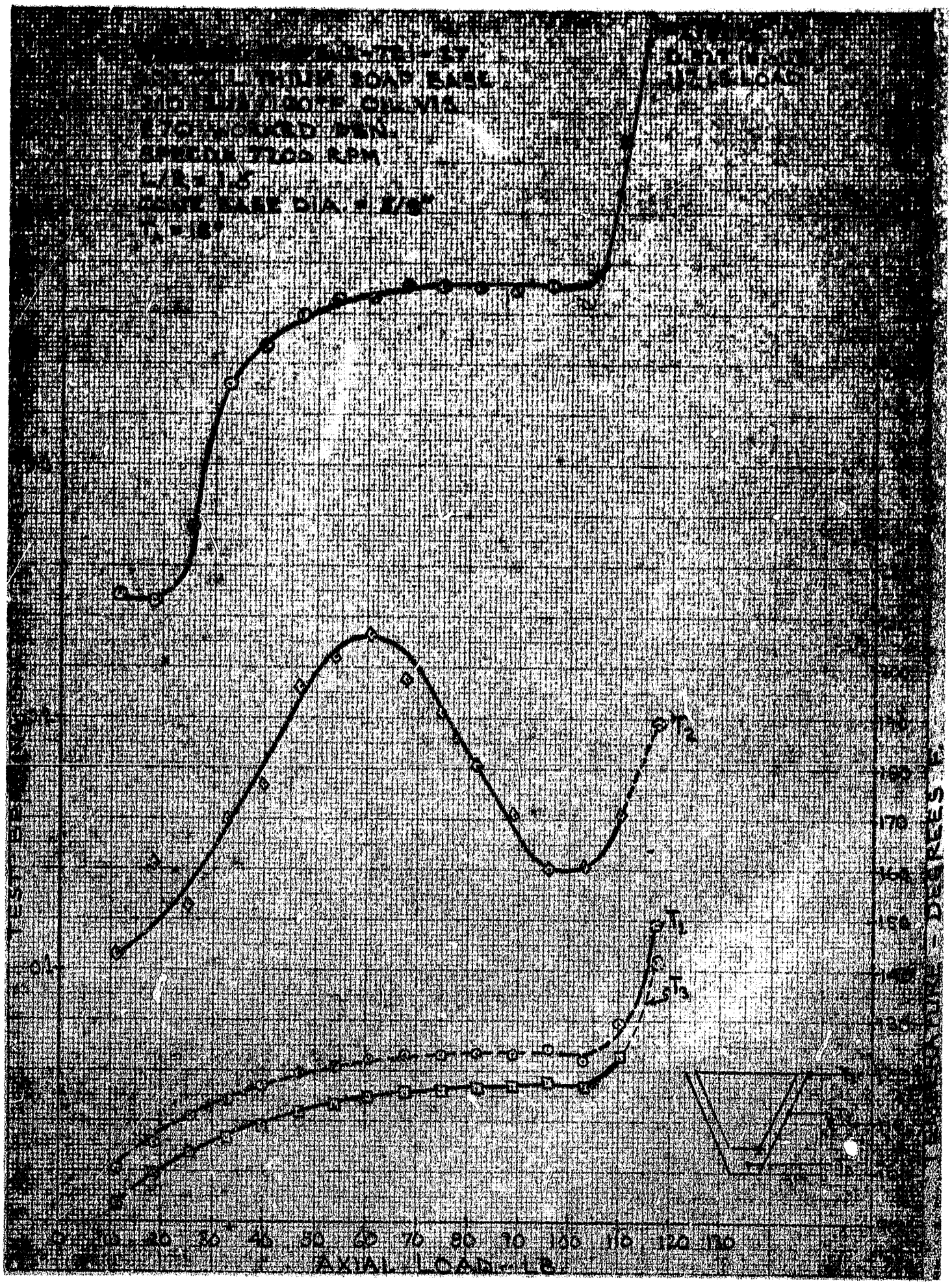

Fig. 7-5

Table 7-1

EXPERIMENTAL RESULTS

CONICAL BEARING SHEAR TORQUE AND LUBRICANT TEMPERATURE WITH 50 LB. AXIAL LOAD ON 5/8" DIA. X 15/32" LONG CONE

Lubricant Type	Torque In. Lb	Temp. T_2^* °F	Worked Pen.	% Weight of Soap	Type Soap	Oil Vis. SUS/100°; SUS/210°	Max. Thrust Load-Lb	Comments
X-721-15	0.269	111	340	5.5	Lithium	530,58	174	Best Performance
X-721-16	0.289	114	300	4.7	Al-Complex	515,63	181+	Good Performance
X-721-7	0.302	117	436	2.2	Al-Complex	530,59	181+	Poor Self-Sealing Characteristic but Good Load Capacity
X-721-22	0.310	120	324	5.5	Lithium	750,59	181+	Good Load Capacity but High Torque
X-721-27	0.360	199	270	11.2	Lithium	210,45	117	Poor Torque and Temperature Response
X-721-28	0.428	142	292	8.2	Lithium	530,58	90	Very Poor Torque and Temperature Respons
V63	0.248	114	---	---	----------	538,68	104	Newtonian Oil Poor Loading Capacity; not Self-Sealing

* T_2 is Lubricant Temp. at mid-plane of cone

+ Load Capacity exceeds maximum that could be applied (181 lb)

- Base stock - petroleum oil
- Oil viscosity - 200 SUS/100°F; 45 SUS/210°F
- Soap-type-Lithium
- Percent weight of soap - 5
- Worked Penetration (ASTM D217) - 320 to 350
- Dropping point (ASTM D2265) - 380°F

8. EXPERIMENTS WITH THE SIMULATED SPIN AXIS ROTOR SUPPORTED ON GREASE LUBRICATED BEARINGS

8.1 Fabrication of Grooved Conical Journal

To provide a groove geometry that closely approached the idealized analytical model, a machining rather than an etching process was adapted for generating grooves. An additional motivation for this approach was that a precision machining capability was readily available in-house.

Figure 8-1 shows a Bridgeport milling machine with a Precise grinding spindle clamped to the rear end of the ram. The grinding spindle is positioned over the table and fitted with a chuck to hold an end-mill. For the 3/16 in. diameter cone previously described, the end mill is ground to a 7 mil cutting width and rotated at 35,000 rpm. The speed is controlled by the Variac shown on the right hand side of the milling table. The journal to be grooved is mounted in a fixture and secured to a universal dividing head which is tilted to the appropriate angle relative to the end mill axis. The crank handle on the dividing head is used to index the cone, thus determining the number of spiral grooves. When the locking pin is removed from the index plate, manual rotation of the crank handle causes the cone to rotate about its axis. At the same time, the milling table is translated horizontally by the compounded gearing which couples the dividing head to the table lead screw. This gearing ratio determines the groove angle α. The set-up shown in Figure 8-1 was used to machine the grooves shown in Figure 4-2.

8.2 Balancing Rotor Assembly

The rotor assembly consists of a disc (simulating the gyro wheel) with machined-in turbine buckets and a split shaft that bolts to either side of the disc. A special fixture was constructed to balance the rotor in two planes. Basically, the fixture consists of a yoke, two support bearings and three miniature capacitance probes. The capacitance

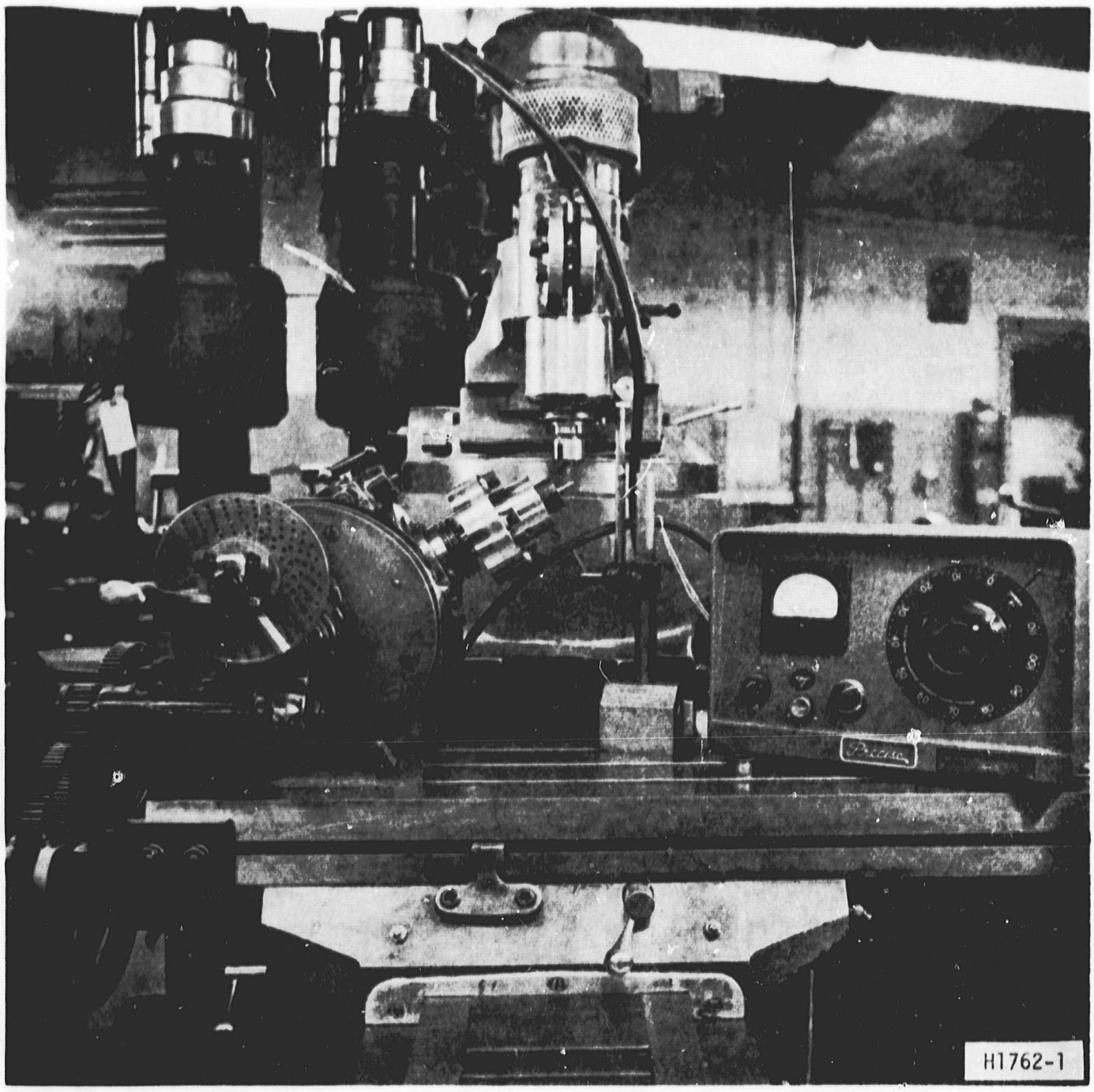

Fig. 8-1 - Milling Set-up to Cut Spiral Grooves on a Conical Surface

probes are connected to Wayne Kerr vibration meters with output displayed on an oscillograph. The rotor support bearings are grease lubricated and identical to those used in the gyro. Each bearing is machined in a rod. The rods have milled flats such that they are flexible in one direction and stiff in the other. The rods are clamped in a split support housing to achieve a predetermined bearing clearance. A capacitance probe is mounted at the mid-plane of each bearing and a third probe faces the wheel to provide a trigger pulse for phase determination. Since there was a slight difference in concentricity between the cones and the shaft, the probes were set to indicate the bearing motion rather than the shaft motion. The two side faces of the disc were selected as balance planes since it was not convenient to balance in the probe planes.

Balance is accomplished as follows:

One probe station (at the mid-plane of one of the cone bearings) is designated station A_p; the other, station B_p. An oscillograph indicates the amplitude of the bearing vibration and its phase angle relative to the trigger pulse. This initial response at A_p is designated by the complex number A_0. A similar reading is taken at station B_p producing an amplitude and phase angle recorded as the complex number B_0. Next, a known mass is placed in balance plane A_b (the side face of the disc nearest probe station A_p). The angle relative to the triggering pulse mark on the disc is recorded. The amplitude and phase angle of the resulting mark on the disc is recorded. The amplitude and phase angle of the resulting vibration in probe stations A_p and B_p are designated as A_{01} and B_{01}.

A third run is made placing a known mass at a known phase angle in balance plane B_B. The vibration response in both probe planes is again recorded and designated A_{02} and B_{02}. A_1 is derived from A_{01} and A_0 by vector subtraction; B_1 is similarly derived. Thus

$$A_1 = A_{01} - A_0, \quad B_1 = B_{01} - B_0$$

and

$$A_2 = A_{02} - A_0 \quad B_2 = B_{02} - B_0$$

Assuming that the displacement is proportional to the mass, the balancing problem reduces to determining the complex operators A and B such that the initial vibration response is cancelled, i.e.,

$$\begin{aligned} A \cdot A_1 + B \cdot A_2 &= -A_0 \\ A \cdot B_1 + B \cdot B_2 &= -B_0 \end{aligned} \tag{8.1}$$

Defining

$$D = \begin{vmatrix} A_1 & A_2 \\ B_1 & B_2 \end{vmatrix}$$

then

$$A = \frac{1}{D} \begin{vmatrix} -A_0 & A_2 \\ -B_0 & B_2 \end{vmatrix}, \qquad B = \frac{1}{D} \begin{vmatrix} A_1 & -A_0 \\ B_1 & -B_0 \end{vmatrix} \tag{8.2}$$

A and B give the magnitude and angle of the correction vectors. The test weight at A_b is multiplied by the magnitude of A; the phase angle of A is added to the angular location of the test weight at A_b. This gives the correction weight and its location for plane A_b. Similarly, the correction for plane B_b is computed. Theoretically, the application of the correction weights should reduce the origional bearing unbalance forces to zero.

The above procedure reduced the original unbalance by about 80%. A further reduction was obtained by repeating the two response measurements with smaller test masses. The residual unbalance was estimated at less than 2×10^{-5} in.-Oz.

8.3 Description of Simulator Rig

The purpose of the Gyro Simulator Test Rig is to provide an accurate device for measuring the performance of a rotor that simulates the specification given in Section 4.1 and is supported on grease or oil lubricated, self-sealing gyro spin asix bearings. Figure 8-2 shows some of the components of the rig that was constructed to meet this objective. The basic design concepts of this test device are:

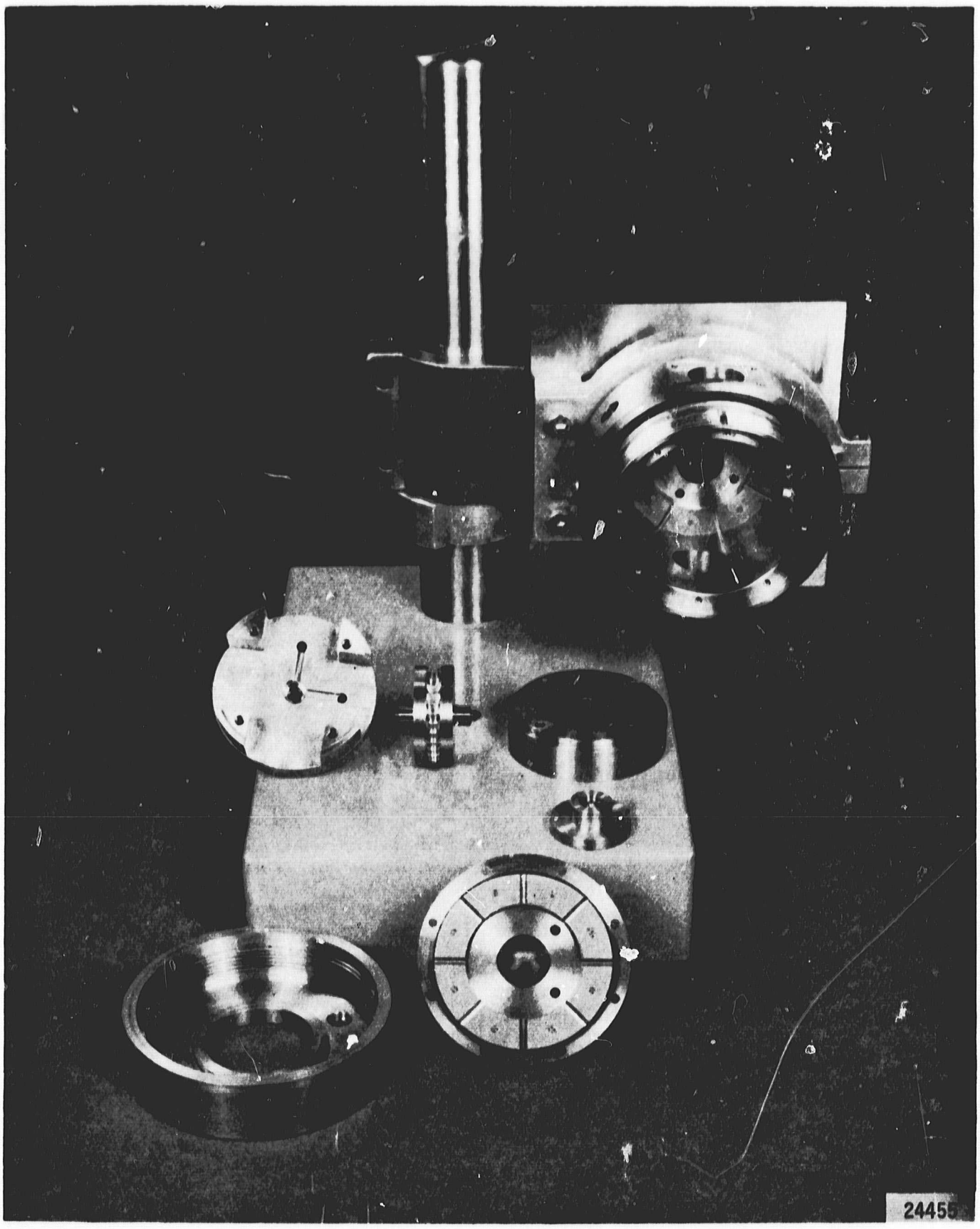

Fig. 8-2 - Gyro Simulator Test Rig with Rotor and Dynamometer Body Disassembled

(a) Bearing friction torque is determined by fixing the test rotor bearings in end plates of an air bearing supported cylinder and measuring the torque required to constrain the cylinders' rotation.

(b) Loads are applied to the test rotor through gas bearing films

(c) Dynamic motions and deflections are measured by non-contacting probes

(d) The rotor axis may be positioned at any angle between vertical and horizontal

(e) Dead weight determines vertical loads; horizontal load and torque are measured by strain gage transducers

(f) Rotor speed is set by turbine nozzle pressure and measured by a photoelectric indicator

The simulated gyro rotor, with a disc diameter of about 2 inches is shown in Figure 8-2 near the center of test stand base plate. Figure 4-2 is a close-up photograph of half of the shaft showing its spiral groove conical end. To the left and right of the rotor in Figure 8-2 are the two sections of the cylindrical dynamometer body. The left bearing, (female cone) together with two orthogonal probe mounting slots, is visible at the center of the dynamometer section located to the left of the rotor. The milled "cross" in this piece provides radial access to the wheel for the radial load piston, the turbine nozzles and the speed counter. The other section of the dynamometer body is called the "cap" and is machined to snap-fit with its mating component. The base of the right hand bearing is visible in the flanged piece placed in the right fore-front of the test stand bed plate. To provide axial loadings, this component is machined to slide in the dynamometer cap. A dowel hole in the bearing flange and a pin through the cap prevents rotation with respect to the dynamometer body.

Clamped to an angle plate and mounted on the test stand column is the dynamometer housing. One of the segmented air lubricated thrust bearings can be seen at the inside rear of this cylindrical housing. The other thrust bearing is placed in front of the test stand in Figure 8-2. The ports in the dynamometer housing are provided for the radial load cell, the turbine nozzle and the speed indicator. The interior cylindrical surfaces on either side of the ports are the journal bearing areas for the dynamometer body. The threaded piece to the left-front of the test stand in Figure 8-2 is one of the gas manifold covers.

Figure 8-3 shows the rear of one of the thrust bearings, which has been bolted to the dynamometer housing and placed at the center of the bed plate. Visible in this view are the 8 thrust bearing orifice inserts and two of the 8 journal bearing orifice inserts. The rear manifold cover is shown clamped to the angle plate.

At the right front of the test stand, the rotor is shown inserted in the dynamometer body. The cylindrical post attached to the dynamometer body pertrudes through the housing assembly and is used to transmit the bearing shear torque to the read-out equipment.

Figure 8-4 shows the assembly with some of the instrumentation attached. To the outside of the left manifold cover can be seen the rear of the torque arm assembly. Connected to the base of the torque arm, and behind the right angle mounting bracket is a strain gage transducer used for test bearing friction read-out.

The radial load is applied by the weight sitting on the platform at the top left of Figure 8-4. The platform screws into the end of a load piston which is supplied air through the fitting shown to the left of the slotted guide tube. The inside end of the load piston has the curvature of the wheel and straddles its buckets with externally pressurized air bearing surfaces. Thus, the load piston does not make metal-to-metal contact with the rotor.

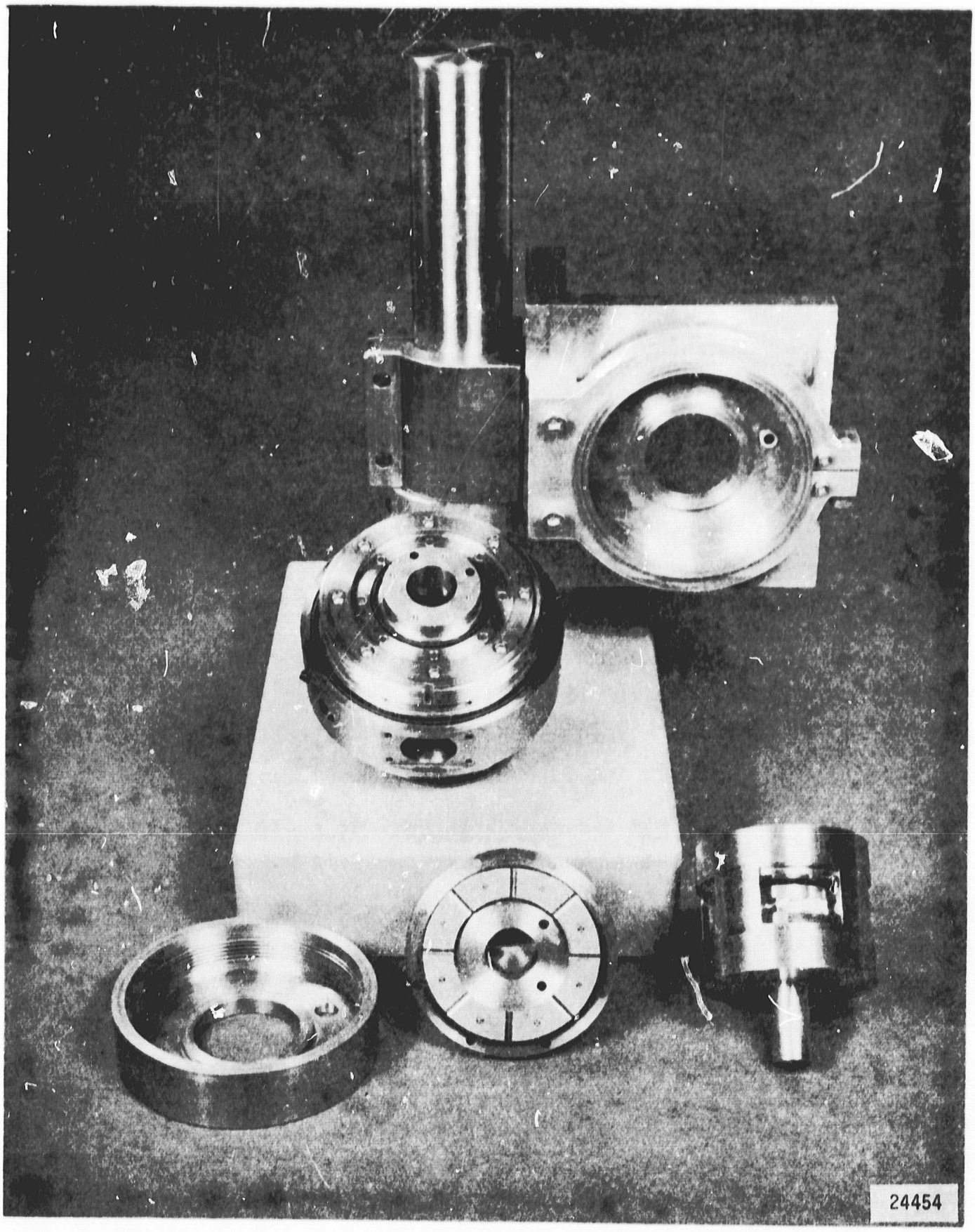

Fig. 8-3 - Gyro Simulator Test Rig with Rotor and Bearings Assembled in Dynamometer Body

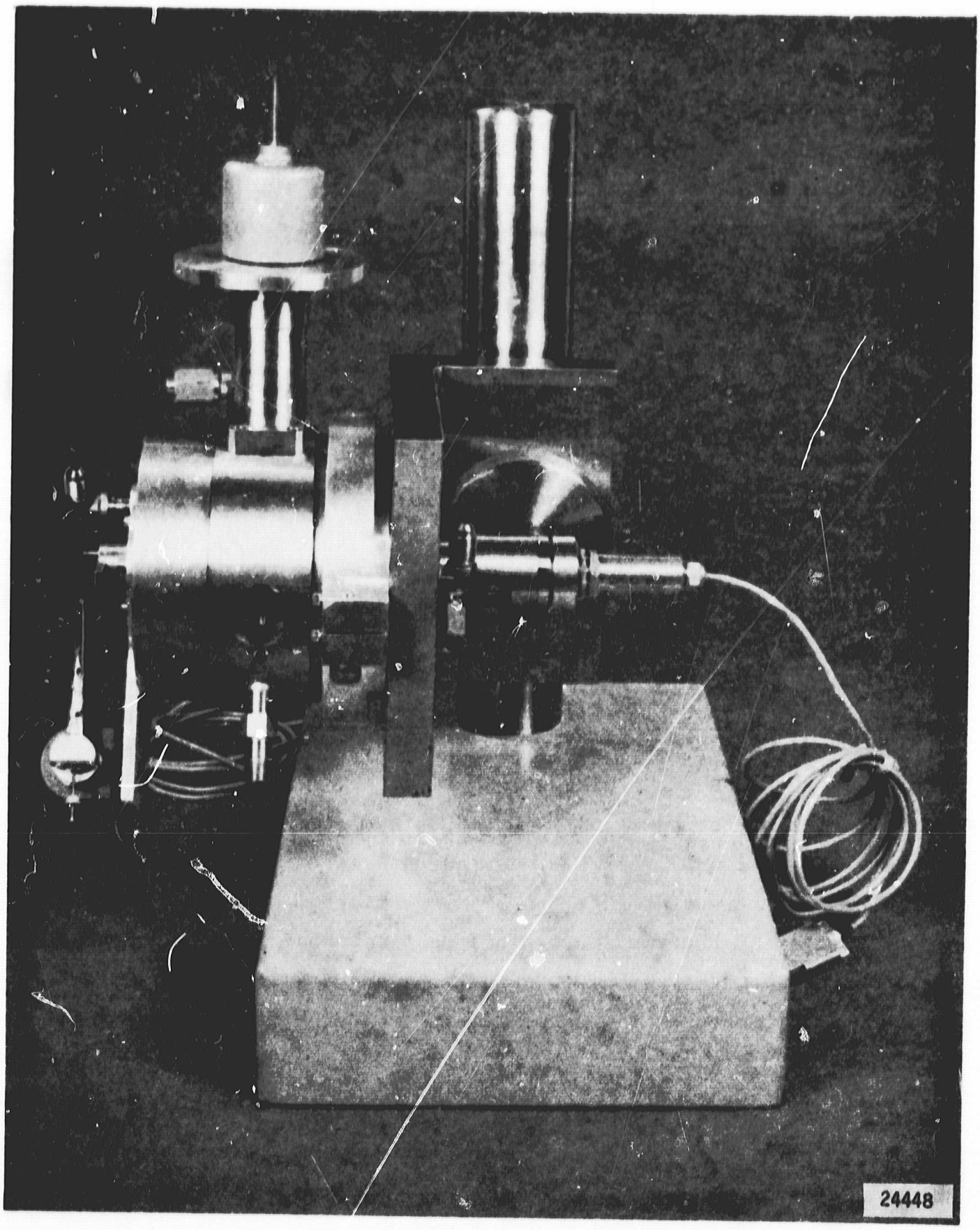

Fig. 8-4 - Gyro Simulator Test Rig Assembled

The axial load is applied through the assembly that pertrudes to the right of the angle bracket in Figure 8-4. This assembly consists of a strain gage transducer with a cord, a load range scaling adapter and a guide tube that bolts to the dynamometer housing. Inside the guide tube is a hollow piston whose air bearing face transmitts an axial force to the test bearing. Turning a differential screw results in a small motion of the axial load piston towards the grease bearing and an opposite motion of the scaling adapter towards the transducer. The transducer read-out records the axial force applied to the grease bearings.

When the test stand angle bracket is rotated so the spin axis is vertical, the dead weight platform and the force transducer assembly are removed and interchanged.

Shop fabrication drawings for the test rig are available and will be transmitted to NASA at the termination of the program.

8.4 Summary of Test Experience

The dynamometer body, containing the simulated gyro rotor, was floated on its gas bearings without experiencing difficulty. The torque read-out system performed as anticipated except that even the most flexible capacitance probe cable available was far too stiff to permit simultaneous readings of dynamic performance and bearing friction torque. To obtain accurate test data, the torque readings must be obtained with the capatance probe cables removed. This situation can be avoided in future designs by mounting the probes to the fixed housing and providing clearance in the dynamometer body.

After the rotor was balanced, its bearings were lubricated with X-721-15 grease (see Table 7-1) and the rotor was installed in the simulator test rig.

With a negligible axial load (corresponding to a concentric clearance of about 0.002 in.) the rotor, in the horizontal orientation, was driven to 30,000 rpm. There was no noticable rig vibration at this

speed. As axial load was slowly applied, the rig began to vibrate. The axial load was increased until, at about 15 lbs, the vibration ceased. The rotor was then running at about 21,000 rpm with no change in the nozzle pressure that originally drove the rotor to 30,000 rpm.

In order to determine the influence of the air bearing films supporting the dynamometer body and separating the axial load piston from the grease bearing, the air to these bearings was cut off and the experiment was repeated. The same dynamical situation was re-encountered with stabilization again occurring at an axial load of about 15 lb. Note that over the projected area of the cone, the average pressure at a 15 lb. axial load is about 540 lb/in.^{2}.

The grooved cones on the rotor were stainless steel; the bearings were leaded bronze. When the rotor was dissembled, minute particles of bronze were observed in the grease lubricant. Also, some score marks were observed on the land area of the rotor cone.

To obtain more information on the dynamical performance of the grease bearings, the rotor was mounted vertically in the balancing fixture which was clamped to the column of the gyro simulator test stand. The bearings were the same as those used in the balancing test runs (see Section 8.2). Two capacitance probes were mounted on either side of the rotor disc to detect axial motion. A third probe was mounted facing the disc and diagonally opposite one of the other probes. This pair of probes was used to detect rotor conical motion. One bearing was free to slide in its housing; the other was fixed. A platform for applying dead weight loading to the sliding bearing was provided. The weight of the platform and top bearing was 0.4 lb and the rotor weighed 0.6 lb. When a 3 lb load was placed on the platform, the rotor ran smoothly at about 20,000 rpm, but when the load was reduced to 2 lb a rotor vibration was encountered. The vibrational mode was almost completely conical with a frequency of about 4000 cpm.

The rotor was restarted and a 5 lb load was placed on the platform. The rotor speed was maintained at 24,000 rpm and the platform load was reduced in one lb increments until a one lb load remained. At a one lb load the rotor showed signs of going in and out of its conical vibrational mode. When only the platform weight was applied to the bearing, the rotor became unstable.

The tests conducted to date indicate that under certain conditions the grease bearing system can become unstable. Much more experimental and analytical work must be undertaken to determine the relations between stability, axial load (or preload), bearing manufacturing tolerances, mounting alignment requirements and lubricant properties. The test experience gained to data indicates that the rotor vibration encountered is *not* a severe design problem. Also, in spite of occasional high over-load, rotor vibration and non-perfect bearing geometry, a catastrophic bearing failure was *never* encountered. The bearings always restarted and developed a full fluid film.

9. REFERENCES

1. Muijdermann, E. A., *Spiral Groove Bearings*, Phillips Technical Library, Springer-Verlog New York Inc.

APPENDIX A

THEORETICAL PERFORMANCE DATA FOR THE SPHERICAL SPIRAL GROOVE BEARING

As one of three prime candidates for the gyro spin axis application, the spherical spiral groove bearing was investigated using the analysis outlined in Section 5.1. Although it looks possible to adapt this configuration to meet the design requirements, the spherical bearing was not selected for experimental evaluation because it was thought that the conical configuration provided more design flexability. For the sake of completeness, some of the theoretical performance data that was obtained is included in this Appendix. Other data may be found in the various monthly progress reports.

Figures A-1 through A-3 show the performance characteristics for a sphere with an infinite number of grooves ($K = \infty$)and a 90 degree groove band ($\psi_1 = 0°$, $\psi_2 = 90°$). Figures A-4 through A-6 show the same characteristics for 7 grooves and a 65 degree groove band ($\psi_1 = 25°$, $\psi_2 = 90°$). Figure A-7 shows the influence of varying ψ_1 and Figure A-8 shows the influence of varying K. See Section 5.1 for nomenclature.

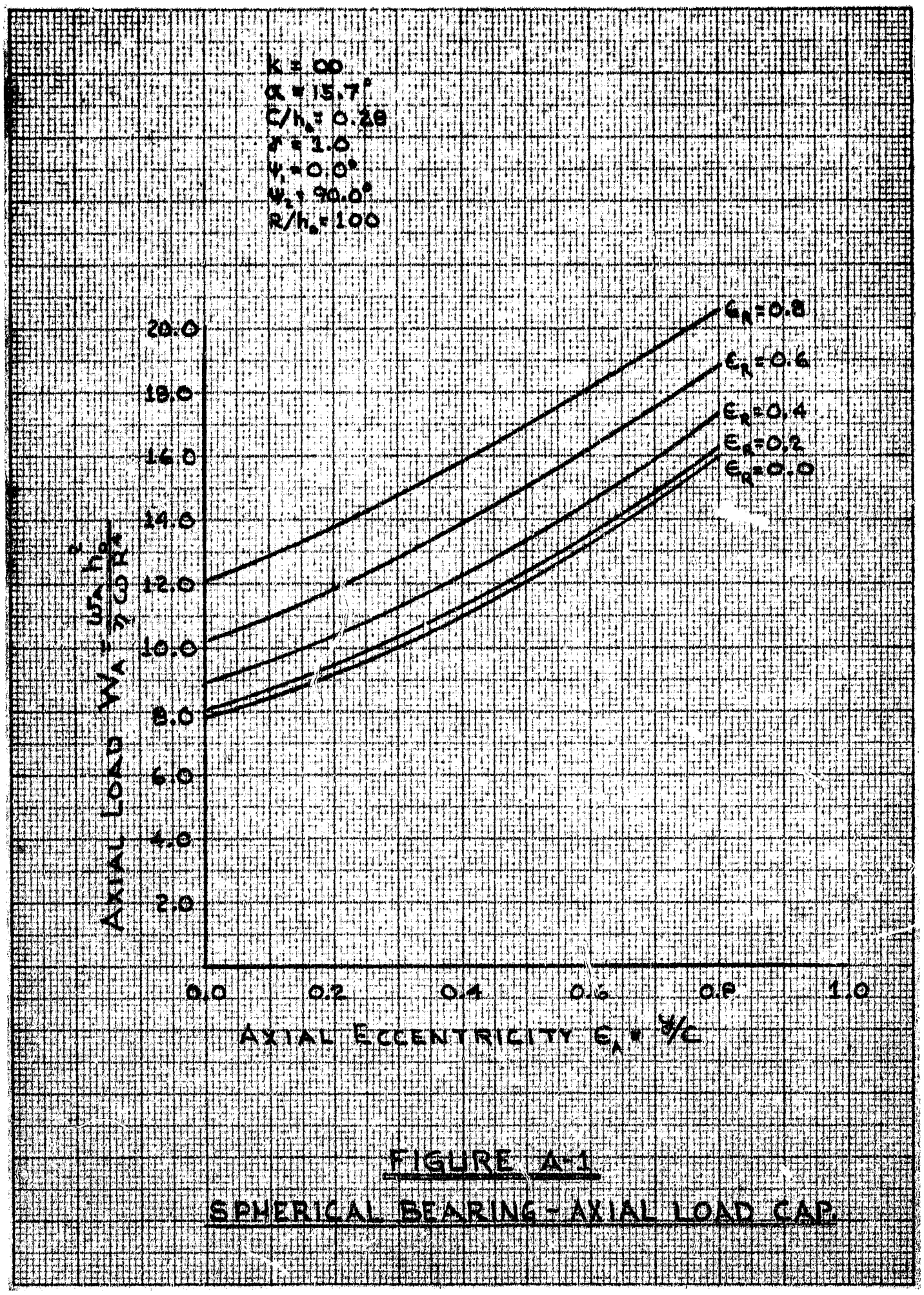

FIGURE A-1

SPHERICAL BEARING - AXIAL LOAD CAP.

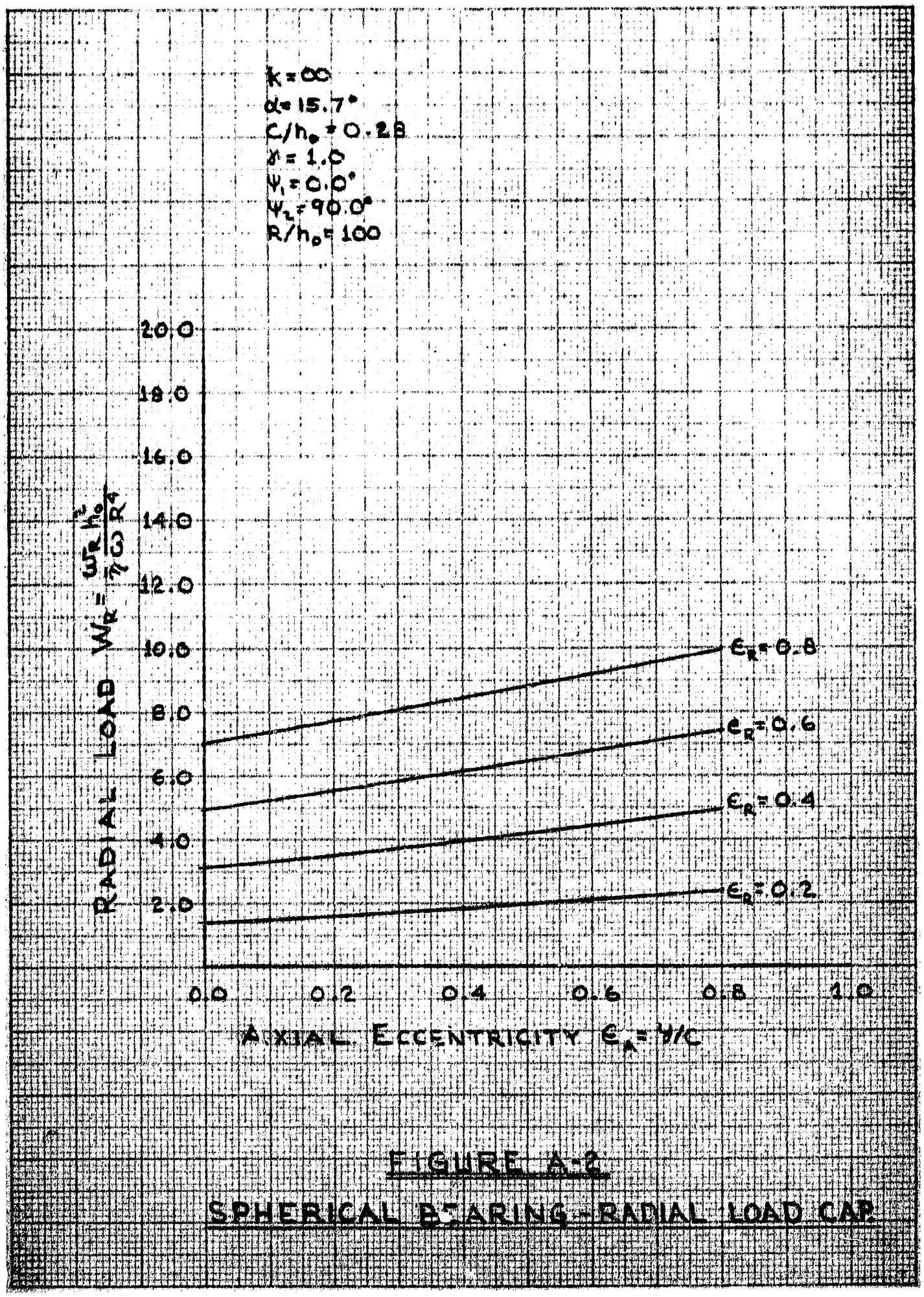

FIGURE A-2

SPHERICAL BEARING - RADIAL LOAD CAP

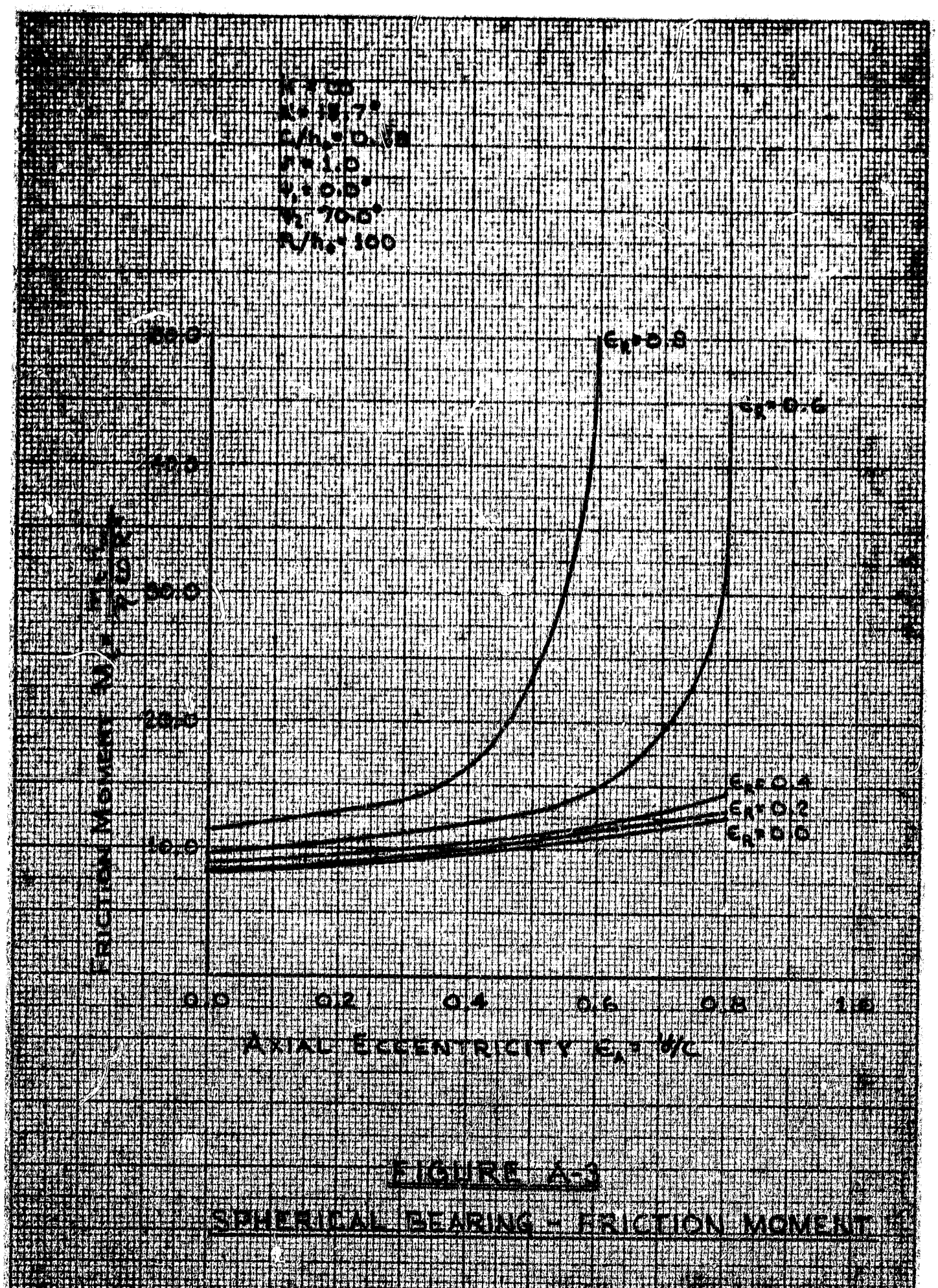

FIGURE A-3

SPHERICAL BEARING - FRICTION MOMENT M

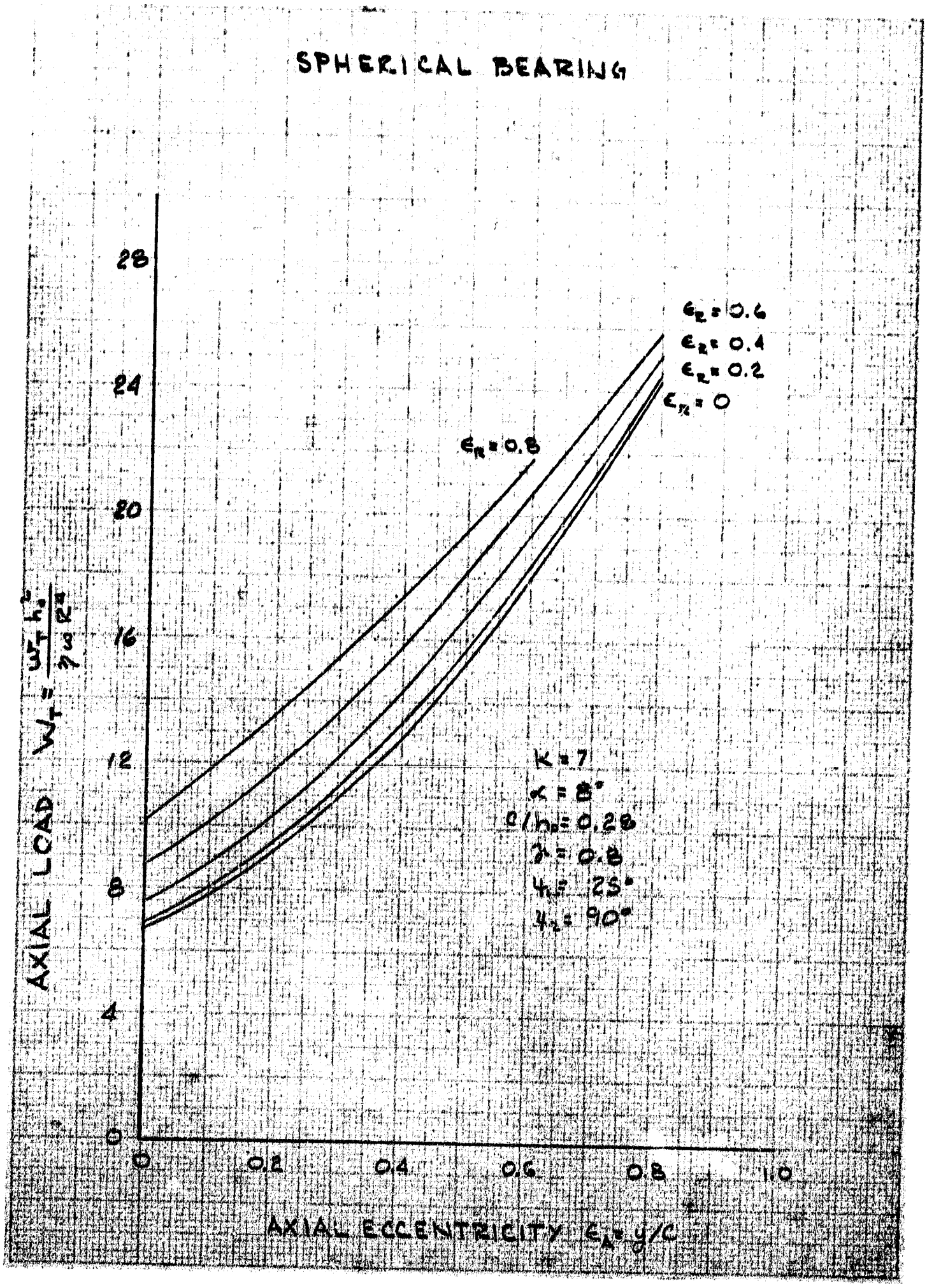
SPHERICAL BEARING
AXIAL LOAD $W_T = \frac{W_T h_o^2}{\gamma_3 R^4}$
28
24
20
16
12
8
4
0
$\epsilon_R = 0.6$
$\epsilon_R = 0.4$
$\epsilon_R = 0.2$
$\epsilon_R = 0$
$\epsilon_R = 0.8$
K = 7
$\kappa = 8°$
$c/h_o = 0.28$
$\lambda = 0.8$
$\psi_1 = 25°$
$\psi_2 = 90°$
0
0.2
0.4
0.6
0.8
1.0
AXIAL ECCENTRICITY $\epsilon_A = y/c$

Fig. A-4

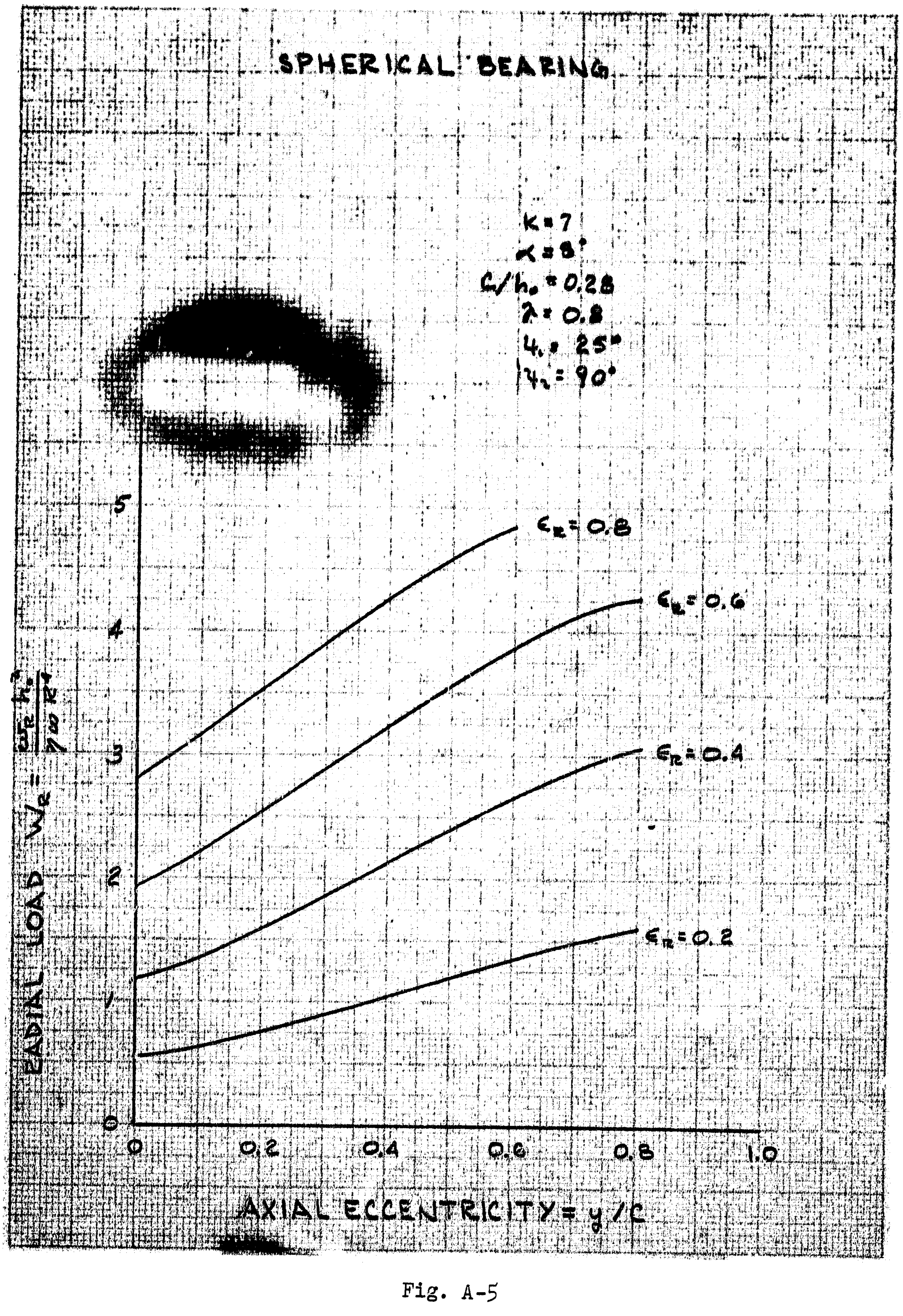

SPHERICAL BEARING
K = 7
α = 8°
C/h₀ = 0.28
λ = 0.8
ψ₁ = 25°
ψ₂ = 90°
ε_R = 0.8
ε_R = 0.6
ε_R = 0.4
ε_R = 0.2
RADIAL LOAD
0
1
2
3
4
5
0
0.2
0.4
0.6
0.8
1.0
AXIAL ECCENTRICITY = y/C

Fig. A-5

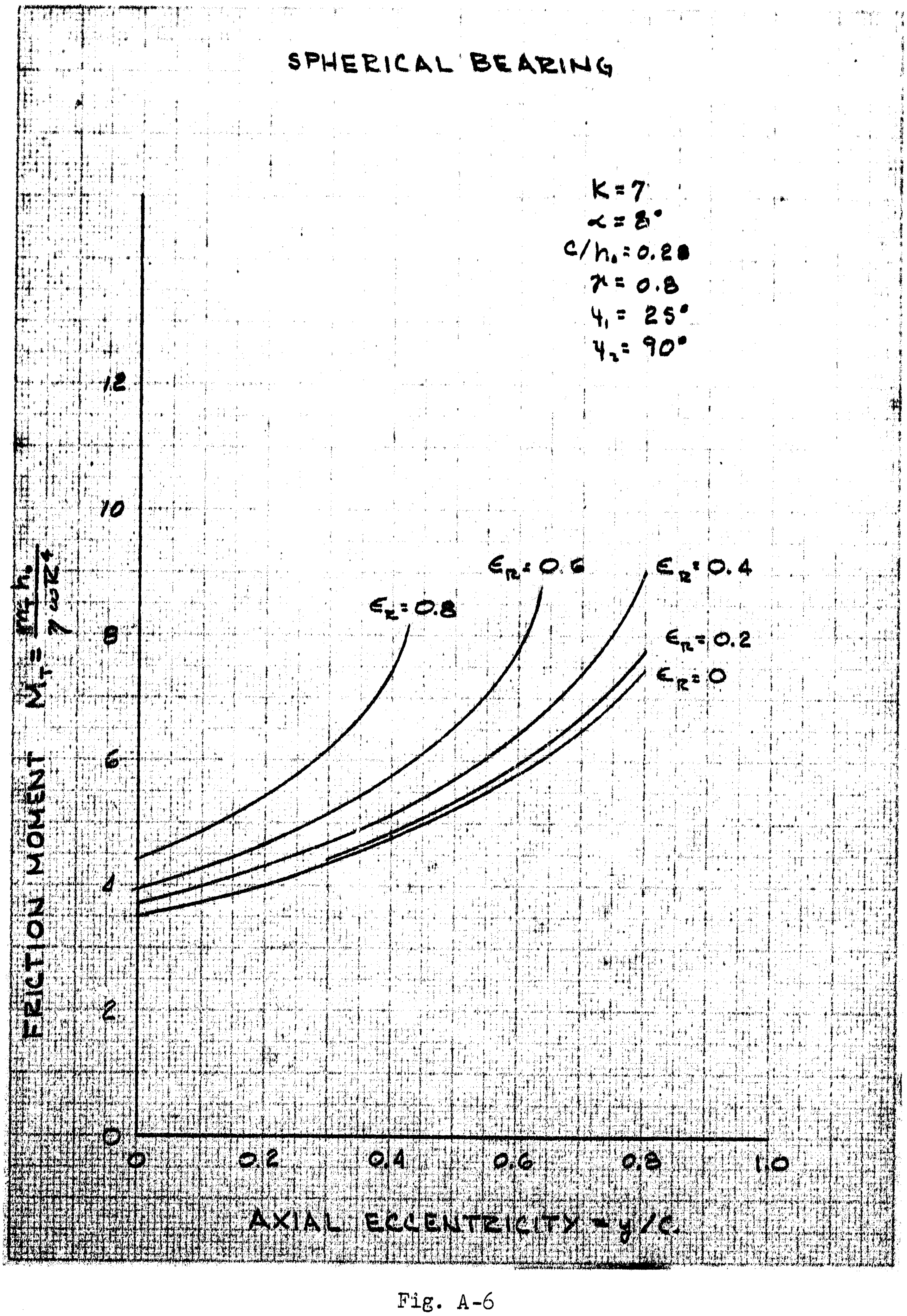
SPHERICAL BEARING
K = 7
α = 8°
C/h₀ = 0.28
λ = 0.8
ψ₁ = 25°
ψ₂ = 90°
ε_R = 0.8
ε_R = 0.6
ε_R = 0.4
ε_R = 0.2
ε_R = 0
FRICTION MOMENT
12
10
8
6
4
2
0
0
0.2
0.4
0.6
0.8
1.0
AXIAL ECCENTRICITY = y/C

Fig. A-6

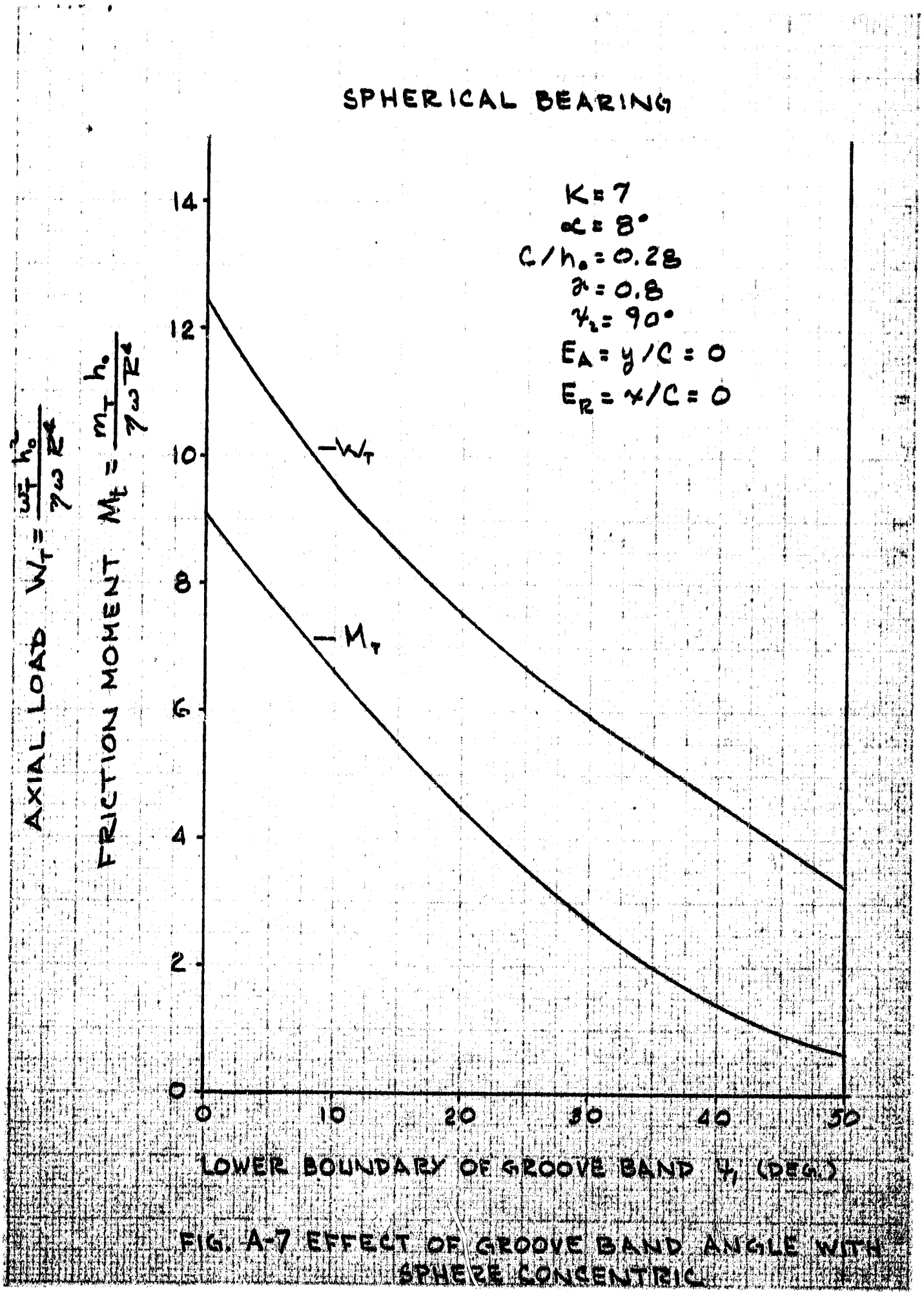

FIG. A-7 EFFECT OF GROOVE BAND ANGLE WITH SPHERE CONCENTRIC

SPHERICAL BEARING

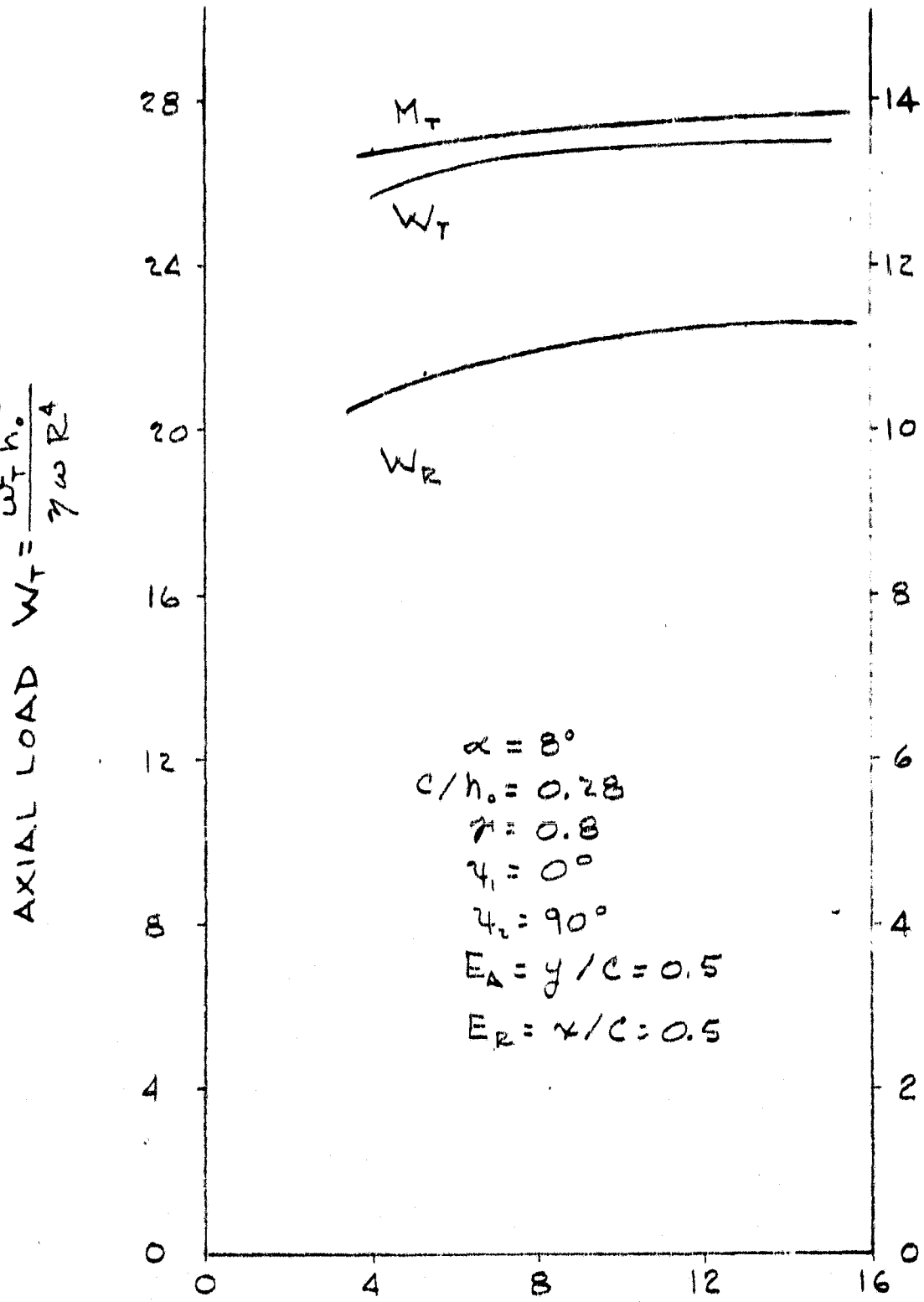

FIG. A-8 EFFECT OF THE NUMBER OF GROOVES WITH SPHERE DISPLACED